



1 Photochemical Degradation of Isoprene-derived 4,1-Carbonyl 2 Nitrate 3

4 F. Xiong¹, C. H. Borca¹, L. V. Slipchenko¹ and P. B. Shepson^{1,2}

5 [1] Department of Chemistry, Purdue University, West Lafayette, IN

6 [2] Department of Earth, Atmospheric and Planetary Sciences, Purdue University, West
7 Lafayette, IN

8 Correspondence to: P. B. Shepson (pshepson@purdue.edu)

9 Abstract

10 In isoprene-impacted environments, carbonyl nitrates are produced from NO₃-initiated isoprene
11 oxidation, which constitutes a potentially important NO_x reservoir. To better understand the fate
12 of isoprene carbonyl nitrates, we synthesized a model compound, *trans*-4-nitrooxy-2-methyl-2-
13 buten-1-al (4,1-isoprene carbonyl nitrate) and investigated its photochemical degradation process.
14 The measured OH and O₃ oxidation rate constants for this carbonyl nitrate are 4.1(±0.7)×10⁻¹¹
15 cm³ molecules⁻¹ s⁻¹ and 4.4(±0.3)×10⁻¹⁸ cm³ molecules⁻¹ s⁻¹. The UV absorption spectrum of the
16 carbonyl nitrate was determined, and the result is consistent with TDDFT calculations. Based on
17 its UV absorption cross section and photolysis frequency in a reaction chamber, we estimate that
18 the ambient photolysis frequency for this compound is 3.1×10⁻⁴ s⁻¹ for a solar zenith angle
19 (SZA) of 45°. The fast photolysis rate and high reactivity toward OH lead to a lifetime of less
20 than one hour for the carbonyl nitrate, with photolysis being a dominant daytime sink. The
21 nitrate products derived from the OH oxidation and the photolysis of the isoprene carbonyl
22 nitrate were identified with an iodide-based chemical ionization mass spectrometer. For the OH
23 oxidation reaction, we quantified the yields of two nitrate products, MVK nitrate and ethanal
24 nitrate, which together contributed to 37(±5)% of the first-generation products.

25 1 Introduction

26 Over the past century, tropospheric ozone concentrations have increased from around 20 ppb to
27 ~40 ppb, with urban-impacted concentrations often rising to 60-100 ppb (Parrish et al., 2014;
28 Vingarzan, 2004), posing harmful effects on human health and crop yields (Lefohn and Foley,



29 1993; Lippmann, 1989). Tropospheric ozone is catalytically produced in the chemical reactions
30 of nitrogen oxides ($\text{NO}_x \equiv \text{NO} + \text{NO}_2$) and volatile organic compounds (VOCs) (Haagen-Smit,
31 1952). NO_2 photolysis forms ozone (Blacet, 1952), and the ozone production rate is enhanced
32 when the $\text{NO-NO}_2\text{-O}_3$ cycle is coupled with the oxidation of VOCs (Chameides et al., 1988;
33 Chameides and Walker, 1973; Chameides et al., 1992). When NO_x is incorporated into organic
34 molecules and forms organic nitrates (RONO_2), however, ozone formation is suppressed
35 (Roberts, 1990). Organic nitrates are a temporary NO_x reservoir. Degradation of organic nitrates
36 can release NO_2 back into the atmosphere (Aschmann et al., 2011), and thus facilitate ozone
37 production. Organic nitrates in the gas phase can also adsorb onto atmospheric aerosols,
38 followed by condensed-phase hydrolysis (Rindelaub et al., 2015). This process removes the
39 reactive nitrogen from the atmosphere permanently, as the nitrooxy group is turned into the non-
40 volatile NO_3^- ion (Darer et al., 2011; Hu et al., 2011). The relative importance of these parallel
41 nitrate sinks affects the availability of NO_x and the ozone production rate in the troposphere.
42 Therefore, detailed understanding of the loss mechanisms of organic nitrates is crucial to
43 understanding the dynamics of ground-level ozone formation.

44 Modeling studies suggest that isoprene-derived organic nitrates have substantial influence on the
45 NO_x cycle and tropospheric O_3 production (Horowitz et al., 2007; Mao et al., 2013; Paulot et al.,
46 2012; Wu et al., 2007). During the daytime, isoprene is lost rapidly to OH oxidation, forming
47 organic nitrates through the $\text{RO}_2 + \text{NO}$ reaction with a yield of 7-14% (Lockwood et al., 2010;
48 Patchen et al., 2007; Paulot et al., 2009; Sprengnether et al., 2002; Tuazon and Atkinson, 1990;
49 Xiong et al., 2015). At night, reaction with NO_3 is a significant removal pathway for isoprene
50 (Brown et al., 2009; Starn et al., 1998), and organic nitrates constitute 65-70% of the oxidation
51 products (Perring et al., 2009; Rollins et al., 2009). While NO_3 -initiated isoprene oxidation
52 contributes to a small fraction of isoprene loss, this reaction pathway could generate
53 approximately half of the isoprene-derived organic nitrates on a regional scale, due to its large
54 nitrate yield (Horowitz et al., 2007; Xie et al., 2013).

55 Fig.1 shows the formation pathways of organic nitrate products from NO_3 -initiated oxidation of
56 isoprene, including hydroperoxy nitrate, carbonyl nitrate and hydroxy nitrate. Reactions for only
57 one of the nitrooxy peroxy radicals are shown for brevity. The hydroxy nitrates can be also
58 formed in the OH-initiated isoprene oxidation reactions, and their production and degradation



59 have been studied extensively in both laboratory and field studies (Chen et al., 1998; Giacobelli
60 et al., 2005; Grossenbacher et al., 2004; Jacobs et al., 2014; Lee et al., 2014b; Lockwood et al.,
61 2010; Patchen et al., 2007; Paulot et al., 2009; Sprengnether et al., 2002; Tuazon and Atkinson,
62 1990; Xiong et al., 2015). For the hydroperoxy nitrates, Schwantes et al. (2015) investigated
63 their production from the $\text{RO}_2 + \text{HO}_2$ reaction and identified the nitrooxy hydroxyepoxide
64 product from the OH oxidation of the isoprene hydroperoxy nitrate. For the isoprene carbonyl
65 nitrates, their formation has been quantified in an experimental study (Kwan et al., 2012), but
66 their sinks and fate can only be inferred from analog molecules, such as nitrooxy ketones, due to
67 lack of direct studies on these specific compounds. Suarez-Bertoa et al. (2012) conducted
68 kinetics experiments on three synthesized saturated nitrooxy ketones, and their results indicate
69 that photolysis is the dominant sink for these nitrate compounds. By comparing the published
70 UV absorption spectra of α -nitrooxy ketones with the UV spectra of the mono-functional nitrates
71 and ketones, Müller et al. (2014) suggested that the nitrooxy ketones have enhanced absorption
72 cross sections, which can facilitate the dissociation of the O-NO₂ bond. Like the nitrooxy
73 ketones discussed by Suarez-Bertoa et al. (2012) and Müller et al. (2014), the carbonyl nitrate
74 derived from NO₃ + isoprene oxidation has a chromophore, -C=C-C=O, at the β position of the
75 nitrate group, which may enhance the UV absorption cross section of the molecule and facilitate
76 its photolytic dissociation. However, since the five-carbon isoprene carbonyl nitrate (Fig. 1) is
77 unsaturated, it is expected to be lost rapidly to OH oxidation. To date, the relative importance of
78 the individual photochemical sinks for the unsaturated carbonyl nitrates is still unclear. To
79 answer this question, we synthesized a model compound for the five-carbon isoprene carbonyl
80 nitrates, and investigated its photochemical reactivities.

81 **2 Synthesis and characterization**

82 A model compound, 4,1-isoprene carbonyl nitrate (*trans*-2-methyl-4-nitrooxy-2-buten-1-al) was
83 synthesized following the reaction scheme in Fig. 2. The nitrate was prepared by reacting AgNO₃
84 with the corresponding bromide (*trans*-4-bromo-2-methyl-2-buten-1-al) (Ferris et al., 1953),
85 which was synthesized following Gray (1981). The ¹H and ¹³C NMR spectra of the synthesized
86 product are shown in Fig. S1 and Fig. S2. Its IR absorption spectrum is shown in Fig. S3.



87 Shown in Fig. 3 are the UV absorption cross sections for the carbonyl nitrate, methacrolein
88 (MACR) and isopropyl nitrate, obtained in acetonitrile solvent. The absorption cross section of
89 the carbonyl nitrate is enhanced relative to that of MACR, but the two spectra have similar
90 features from 320 nm to 400 nm with peak absorption at 325 nm. This is probably because they
91 both contain the O=C–C=C chromophore. Below 320 nm the absorption of the carbonyl nitrate is
92 enhanced significantly in comparison with that of isopropyl nitrate. This observation is
93 consistent with reports from Müller et al. (2014) that molecules containing α,β -nitrooxy ketone
94 functionalities have enhanced UV absorption.

95 **3 Methods**

96 **3.1 Setup for the kinetics chamber experiments**

97 Three sets of reaction chamber experiments were conducted to determine the photolysis
98 frequency, OH oxidation rate constant and the O₃ oxidation rate constant for the carbonyl nitrate.
99 The experiments were performed in the 5500 L Purdue photochemical reaction chamber (Chen et
100 al., 1998). A chemical ionization mass spectrometer (CIMS) with I⁻ as the reagent ion was used
101 to quantify the carbonyl nitrate and its nitrate degradation products (Xiong et al., 2015). The
102 chamber air was sampled into the CIMS through a 5.2 m long FEP tubing (0.8 cm ID, heated to
103 constant 50 °C). The photolysis frequency was obtained by measuring the loss of the carbonyl
104 nitrate inside the reaction chamber in the presence of UV radiation and propene as a radical
105 scavenger. When the UV lamps were turned off, the wall loss rate constant for the carbonyl
106 nitrate was derived by observing its slow decay, with propene as an ozone and NO₃ scavenger.
107 The OH reaction rate constant and O₃ reaction rate constant were obtained using the relative rate
108 method (Atkinson and Aschmann, 1985). Propene was used as the reference compound, and its
109 changing concentrations were measured using a GC-FID equipped with a 0.32 mm Rtx-Q-Bond
110 column. For the OH oxidation experiments, OH was generated through the photolysis of
111 isopropyl nitrite, which was synthesized following Noyes (1933). NO was added to the chamber
112 to suppress the formation of O₃. In addition, two OH oxidation experiments were performed
113 without propene in order to quantify the oxidation products. For the OH-initiated oxidation
114 experiments, NO and NO₂ were measured using the Total REactive Nitrogen Instrument
115 (TRENI) (Lockwood et al., 2010). The ozonolysis experiments were performed in the dark, and



116 cyclohexane was added to the chamber as an OH scavenger. The initial conditions for the
117 experiments are listed in Table S1.

118 **3.2 Computational methods**

119 The theoretical UV absorption spectra of the carbonyl nitrate, MACR, and *n*-butyl nitrate in the
120 gas phase were calculated and analyzed, in four stages, using time-dependent density functional
121 theory (TDDFT; Hohenberg and Kohn, 1964; Kohn and Sham, 1965; Runge and Gross, 1984).
122 All calculations were carried out using the computational chemistry package Q-Chem 4.3 (Shao
123 et al., 2015). First, the structure of each molecule was optimized employing the long-range
124 corrected hybrid density functional ω B97X-D (Chai and Head-Gordon, 2008) with the 6-31+G*
125 basis set (Frisch et al., 1984). A high accuracy grid was employed. Second, frequencies
126 calculations were executed on the optimized structures to verify their accuracy. These were run
127 using the same setup described above. Third, after assuring the structures represented adequate
128 minima, the first ten singlet excited states of each molecule were computed with TDDFT, using
129 the same functional and basis set. Finally, a visual analysis of the molecular orbitals (MOs) was
130 carried out with the visualization software IQmol 2.7 (Gilbert, 2012).

131 **4 Results**

132 **4.1 Absorption spectra and density functional calculations**

133 Fig. 4 shows the TDDFT UV absorption spectra of the carbonyl nitrate, MACR, and *n*-butyl
134 nitrate. There are three groups of transitions in the simulated spectra.

135 Both MACR and the carbonyl nitrate show a relatively weak transition in the region around 330
136 nm, which corresponds to the first electronic transition, from the highest occupied molecular
137 orbital (HOMO) to the lowest unoccupied molecular orbital (LUMO), in both molecules. Fig. 5a
138 provides comparative information between the first electronic transition of the carbonyl nitrate
139 and the homologous excitation of MACR. As shown in Fig. 5a the character of the molecular
140 orbitals involved in this transition is similar in both cases, indicating that the aldehyde group is
141 involved in the first electronic excitation of the carbonyl nitrate.



142 Fig. 5b shows the information corresponding to the second electronic transition of the carbonyl
143 nitrate and the homologous excitation of *n*-butyl nitrate. Both transitions are found in the region
144 around 255 nm, and they are 3 orders of magnitude darker than those at 330 nm. Inspection of
145 the character of the MOs involved in these processes reveals a correspondence between the
146 second electronic excitation of the carbonyl nitrate, HOMO-2 → LUMO+1, and the HOMO →
147 LUMO transition of *n*-butyl nitrate. As with the previous case, that observation confirms that the
148 nitrate group is involved in the second electronic excitation of the carbonyl nitrate, but at
149 wavelengths shorter than present at the Earth's surface. Fig. 5b also shows that in this case, the
150 local character of the MOs involved in the transition is even more pronounced, with bulky lobes
151 placed mainly over the nitrate group.

152 Even though the second electronic transition of carbonyl nitrate is not displayed in the
153 experimental spectra of Fig. 3, because its range covers from 280 nm to 410 nm, it is reasonable
154 to assume that it is caused by the local excitation of the nitrate group, based on the computational
155 results. Thus, it can be suggested that the experimental UV absorption spectra of isopropyl
156 nitrate is comparable to that of *n*-butyl nitrate simulated computationally. Thus it is possible that
157 the feature in the region around 280 nm of the carbonyl nitrate experimental spectrum of Fig. 3
158 could be caused by a broadening of the transition located around 255 nm.

159 The brightest transition in the modeled spectra of the carbonyl nitrate, 3 orders of magnitude
160 brighter than the ones at 330 nm, is located around 210 nm. There are two transitions in this
161 region and each one has a homologous excitation: the HOMO-1 → LUMO in carbonyl nitrate is
162 similar to HOMO-1 → LUMO in MACR, and the HOMO-5 → LUMO+1 in carbonyl nitrate is
163 related to the (mainly) HOMO-1 → LUMO transition of *n*-butyl nitrate. These transitions are
164 beyond the range of the experimental spectra on Fig. 3 and beyond the atmospherically relevant
165 absorption wavelengths.

166 **4.2 Photochemical sinks of 4,1-carbonyl nitrate**

167 Fig. 6 shows the first-order wall loss and photolysis loss of the carbonyl nitrate inside the
168 reaction chamber. The wall loss rate constant was $1.3(\pm 0.1) \times 10^{-5} \text{ s}^{-1}$, and the photolysis rate
169 constant was $3.0(\pm 0.1) \times 10^{-5} \text{ s}^{-1}$, after subtracting the wall loss rate constant from the first-order
170 decay rate constant measured for the photolysis experiments. It is worth mentioning that our



171 reactant carbonyl nitrate has a *trans* configuration, and it may photo-isomerize into the *cis*
 172 configuration, which would be detected at the same m/z by the CIMS. The *cis*-carbonyl nitrate
 173 can either photo-dissociate or isomerize to re-form the *trans* isomer. Our previous work suggests
 174 that the CIMS is 4 times more sensitive to the *cis* configuration than the *trans* configuration
 175 (Xiong et al., 2015). If a significant amount of the *cis* isomer was present, the CIMS signal
 176 should resemble a double exponential curve, because the *cis* isomer was being produced and
 177 consumed simultaneously. In an extreme scenario with rapid *trans* \rightarrow *cis* isomerization, the
 178 CIMS signal should increase under radiation, due to the higher sensitivity of the *cis* isomer. For
 179 our carbonyl nitrate photolysis experiments, a single exponential decay in the CIMS signal was
 180 observed, indicating insignificant contribution from the *cis* isomer. Hence, our measured
 181 photolysis frequency should well characterize the loss rate of the carbonyl nitrate inside the
 182 reaction chamber.

183 Since the UV radiation inside the reaction chamber is different from the UV radiation in the
 184 ambient environment (Fig. 7), Cl_2 was used as a reference compound to extrapolate the nitrate
 185 photolysis rate from chamber radiation to solar radiation. The photolysis decay of Cl_2 in the
 186 reaction chamber was measured with the CIMS (Neuman et al., 2010). Cyclohexane was added
 187 to the chamber to scavenge the Cl atoms so that Cl_2 was not re-formed from $\text{Cl} + \text{Cl}$
 188 recombination. The first-order photolysis rate constant for Cl_2 was $2.50(\pm 0.04) \times 10^{-4} \text{ s}^{-1}$ (Fig.
 189 S4).

190 The photolysis frequency (J) is the integrated product of quantum yield (Φ), absorption cross
 191 section (σ , cm^2) and actinic flux (F , $\text{cm}^{-2} \text{ s}^{-1}$) across all wavelengths (Eq. 1). Therefore, the
 192 photolysis frequencies for the carbonyl nitrate and Cl_2 in the reaction chamber can be compared
 193 as in Eq. 2.

$$194 \quad J = \int \Phi_{\lambda} \sigma_{\lambda} F_{\lambda} d\lambda \quad (\text{Eq. 1})$$

$$195 \quad \frac{J_{\text{Cl}_2}^{\text{chamber}}}{J_{\text{nitrate}}^{\text{chamber}}} = \frac{\sum \Phi_{\text{Cl}_2} \sigma_{\text{Cl}_2} F_{\text{chamber}}}{\sum \Phi_{\text{nitrate}} \sigma_{\text{nitrate}} F_{\text{chamber}}} \quad (\text{Eq. 2})$$

196 $J_{\text{Cl}_2}^{\text{chamber}}$ and $J_{\text{nitrate}}^{\text{chamber}}$ are the photolysis frequencies of Cl_2 and the carbonyl nitrate inside the
 197 chamber. σ_{Cl_2} and σ_{nitrate} are the cross sections for Cl_2 and the carbonyl nitrate at each



198 wavelength. $\sigma_{nitrate}$ was determined by this work (Fig. 3). σ_{Cl_2} has been measured previously
 199 and the IUPAC recommended values were used (Atkinson et al., 2007). $F_{chamber}$ is the
 200 wavelength-dependent flux of photons inside the chamber. The radiation spectrum (Fig. 7) of the
 201 chamber UV lamps (UVA 340) was obtained from the manufacturer (Q-lab), but the actual
 202 absolute radiation intensity in the chamber is expected to differ from the manufacturer's
 203 radiation spectrum by a scaling factor, because of the inverse-square dependence on distance,
 204 and our specific multi-lamp geometry. When Cl_2 was used as a reference compound for the
 205 nitrate photolysis rate, the scaling factors in Eq. 2 will cancel.

206 The Cl-Cl bond dissociation energy is 243 kJ/mol (Luo, 2007a), equivalent to a photon at 492
 207 nm. Since Cl_2 has only one bond, it has unity quantum yield below 492 nm and zero quantum
 208 yield above 492 nm. The emission spectrum of the UV lamps for the reaction chamber is
 209 centered from 300 nm to 400 nm (Fig. 7). Hence, $\varphi_{Cl_2} = 1$ in Eq. 2, at all wavelengths. For the
 210 carbonyl nitrate, however, its quantum yield is affected by the bond dissociation energy,
 211 intramolecular vibrational energy redistribution and relaxation of the excited molecule from
 212 collisions, so an average effective quantum yield ($\varphi_{nitrate}^{eff}$) is assumed, and Eq. 2 becomes Eq. 3.
 213 Since the photolysis rates, absorption cross sections and chamber radiation spectrum were known,
 214 we calculated that $\varphi_{nitrate}^{eff}$ was 0.48.

$$215 \quad \frac{J_{Cl_2}^{chamber}}{J_{nitrate}^{chamber}} = \frac{\sum \sigma_{Cl_2} F_{chamber}}{\varphi_{nitrate}^{eff} \sum \sigma_{nitrate} F_{chamber}} \quad (\text{Eq. 3})$$

216 The effective quantum yield of 0.48 indicates that when the carbonyl nitrates absorbs a photon
 217 inside the reaction chamber, the probability (averaged across the absorption wavelengths) for it
 218 to dissociate is 48%. However, the probability for nitrate photolysis is not equal at all
 219 wavelengths, the low energy photons (long wavelength) being less likely to induce photo-
 220 dissociation. Hence, we introduced a threshold wavelength λ_0 , for which the carbonyl nitrate has
 221 unity quantum yield below λ_0 and zero quantum yield above λ_0 . Although this approach accounts
 222 for the energy difference of photons with different wavelengths, it is still a very rough
 223 estimation. Using the threshold wavelength, the effective quantum yield can be expressed by Eq.
 224 4 and Eq. 5, where $\varphi(\lambda)$ is the quantum yield of the carbonyl nitrate, and $F(\lambda)$ is the chamber



225 photon flux (Fig. 7), as a function of the wavelength λ . Solving for the unknown λ_0 in Eq. 5, we
226 calculated that λ_0 was 347 nm.

$$227 \quad \varphi(\lambda) = \begin{cases} 1 & (\lambda \leq \lambda_0) \\ 0 & (\lambda > \lambda_0) \end{cases} \quad (\text{Eq. 4})$$

$$228 \quad \frac{\sum_{\lambda} F(\lambda) \cdot \varphi(\lambda)}{\sum_{\lambda} F(\lambda)} = 0.48 \quad (\text{Eq. 5})$$

229 The solar radiation spectrum was calculated with the TUV model (Madronich and Flocke, 1998).
230 By assuming that the carbonyl nitrate has zero quantum yield above 347 nm and unity quantum
231 yield below 347 nm, its photolysis frequency is $2.6 \times 10^{-4} \text{ s}^{-1}$ for a solar zenith angle (SZA) of
232 45° , and $3.7 \times 10^{-4} \text{ s}^{-1}$ for SZA of 0° . It is worth mentioning that the condensed-phase and gas-
233 phase absorption spectra should be different, because the solvent molecules affect the
234 polarization and dipole moment of the solute (Bayliss and McRae, 1954; Braun et al., 1991;
235 Linder and Abdunur, 1971). Although we were unable to measure the gas-phase cross section of
236 the carbonyl nitrate, we could assess the uncertainty caused by using the condensed-phase
237 spectrum in our calculation, by comparing the gas-phase and condensed-phase spectra of MACR
238 and isopropyl nitrate (Fig. S5a). On average, the gas-phase absorption cross sections of MACR
239 and isopropyl nitrate are 1.7 times those in the solution phase (Fig. S5b). For the carbonyl nitrate,
240 if the gas-phase cross section is assumed to be 1.7 times that of the solution-phase cross section,
241 the calculated effective quantum yield becomes 0.28, leading to a threshold wavelength (λ_0) of
242 336 nm. Using this set of cross section and quantum yields, we calculated that the nitrate
243 photolysis frequency was $3.1 \times 10^{-4} \text{ s}^{-1}$ for SZA of 45° , and $4.6 \times 10^{-4} \text{ s}^{-1}$ for SZA of 0° , which are
244 19% and 24% larger than results obtained using the condensed-phase cross section. The
245 calculated ambient photolysis frequency is not affected as significantly by the change in the
246 absorption cross section, because it is constrained by the measured photolysis frequency in the
247 reaction chamber. When a larger cross section is applied, a smaller quantum yield is derived, and
248 the calculated ambient photolysis frequency, being the integrated product of the cross section,
249 quantum yield and radiation, will not increase as much as the cross section. In addition to the
250 cross section, our treatment of the wavelength-dependent quantum yield can also introduce
251 uncertainty to the calculated results. If a constant effective quantum yield is used in the
252 calculation, the ambient photolysis frequency is $2.0 \times 10^{-4} \text{ s}^{-1}$ for SZA of 45° , and $2.8 \times 10^{-4} \text{ s}^{-1}$ for



253 SZA of 0° , which are 23% and 24% lower than assuming a threshold wavelength. Therefore, our
254 calculated ambient photolysis frequency, based on condensed-phase absorption cross section and
255 a threshold energy for unity quantum yield, has an uncertainty of 25%. Since we believe that the
256 cross sections are indeed larger in the gas phase, our best estimate is $3.1 \times 10^{-4} \text{ s}^{-1}$ for SZA= 45° .

257 Fig. 8 shows the results for the relative rate experiments for the OH-initiated and O₃-initiated
258 oxidation of the carbonyl nitrate, with propene as the reference compound. The loss of the
259 carbonyl nitrate to wall uptake and photolysis is corrected when comparing the oxidative loss of
260 the nitrate to that of propene, using the same method as Hallquist et al. (1997). The OH and O₃
261 oxidation rate constants for propene are $3.0(\pm 0.5) \times 10^{-11} \text{ cm}^3 \text{ molecules}^{-1} \text{ s}^{-1}$ (Klein et al., 1984;
262 Zellner and Lorenz, 1984) and $1.00(\pm 0.06) \times 10^{-17} \text{ cm}^3 \text{ molecules}^{-1} \text{ s}^{-1}$ (Herron and Huie, 1974;
263 Treacy et al., 1992). These are the IUPAC preferred rate constants for T=298K
264 (<http://iupac.pole-ether.fr/>). Hence, the OH and O₃ oxidation rate constants for the isoprene
265 carbonyl nitrate are, based on the results from the relative rate experiments, $4.1(\pm 0.7) \times 10^{-11} \text{ cm}^3$
266 $\text{molecules}^{-1} \text{ s}^{-1}$ and $4.4(\pm 0.3) \times 10^{-18} \text{ cm}^3 \text{ molecules}^{-1} \text{ s}^{-1}$ respectively, at 295 K.

267 The OH oxidation rate constant for the carbonyl nitrate can be estimated through the structure-
268 activity-relationship (SAR) approach proposed by Kwok and Atkinson (1995). The rate constant
269 for OH addition to the double bond can be calculated as $k(-\text{CH}=\text{CH})$, which is $8.69 \times 10^{-11} \text{ cm}^3$
270 $\text{molecules}^{-1} \text{ s}^{-1}$, multiplied by the two correction factors C(-CHO) and C(-CH₂ONO₂), which are
271 0.34 and 0.47 respectively. The resulting OH addition rate constant is $1.39 \times 10^{-11} \text{ cm}^3$
272 $\text{molecules}^{-1} \text{ s}^{-1}$. The rate constant for H abstraction from the -CHO group is $1.61 \times 10^{-11} \text{ cm}^3$
273 $\text{molecules}^{-1} \text{ s}^{-1}$, after multiplying a correction factor of 1 for having a double bond at its α
274 position. The rate constant for H abstraction from the methylene group is $3.7 \times 10^{-14} \text{ cm}^3$
275 $\text{molecules}^{-1} \text{ s}^{-1}$, calculated by multiplying the base rate constant for methylene groups, which is
276 $9.34 \times 10^{-13} \text{ cm}^3 \text{ molecules}^{-1} \text{ s}^{-1}$, by the correction factors of the nitrate group and the double
277 bond, which are 0.04 and 1, respectively. OH addition to the nitrate group has a rate constant of
278 $4.4 \times 10^{-13} \text{ cm}^3 \text{ molecule}^{-1} \text{ s}^{-1}$, after taking account of the enhancement factor of 1.23 for the
279 methylene group. H abstraction from the methyl group has a rate constant of $1.36 \times 10^{-13} \text{ cm}^3$
280 $\text{molecules}^{-1} \text{ s}^{-1}$. By summing up the rate constants for all these reaction pathways, the SAR-
281 derived OH oxidation rate constant for the 4,1-carbonyl nitrate rate constant is $3.1 \times 10^{-11} \text{ cm}^3$
282 $\text{molecules}^{-1} \text{ s}^{-1}$, approximately 30% lower than the experimental measurement. The dominant



283 reaction channels are OH addition to the double bond and H abstraction from the aldehyde
284 group. Contributions from the other reaction pathways are small (<3%).

285 The relative importance of the three photochemical sinks, photolysis, OH oxidation and O₃
286 oxidation, depends on the solar radiation and the concentrations of OH and O₃. To better
287 illustrate their relative contributions, observations of OH and O₃ from previous field campaigns
288 were used to calculate the loss rates of the carbonyl nitrate. The local solar radiation was
289 calculated with the TUV model (Madronich and Flocke, 1998), which was then used to derive
290 the photolysis frequency. The calculated results (Fig. 9) suggest that photolysis is a significant
291 degradation pathway for the carbonyl nitrate, which can dominate over OH oxidation toward
292 mid-day. When the solar radiation intensity is small (such as 6:00 AM for the 1999 SOS
293 campaign), OH oxidation is likely the dominant sink. Due to the fast photolysis and high
294 reactivity toward OH, the photochemical lifetime of the carbonyl nitrate can be as short as less
295 than one hour.

296 **4.3 Degradation products of the 4,1-carbonyl nitrate**

297 **4.3.1 OH oxidation**

298 The products from the OH-initiated oxidation of the 4,1-carbonyl nitrate were observed by the
299 CIMS. The change in the CIMS signals before and after the reaction are illustrated in Fig. 10,
300 along with assignment of some of the molecular structures based on the molecular weight and
301 likely chemistry. The OH-initiated oxidation reaction can proceed through two channels: H
302 abstraction from the aldehyde group and OH addition to the double bond.

303 For the H abstraction pathway, a peroxyacyl nitrate (PAN) product was observed at m/z 349 (Fig.
304 10), which can be formed as shown in Fig. 11. The first-order dissociation rate constant for the
305 PAN compound was determined at room temperature (295 K) using the following method. A
306 100 L Teflon bag containing the air mixture of approximately 1 ppm isopropyl nitrite and 30 ppb
307 4,1-carbonyl nitrate was irradiated, and the PAN compound was formed from OH and NO₂
308 (produced through the photolysis of isopropyl nitrite) reaction with the 4,1-carbonyl nitrate.
309 After 5 min reaction time, the bag was removed from the UV radiation, and NO was injected into
310 the bag to around 4 ppm in concentration. The bag was then sampled simultaneously by the
311 CIMS, which monitored the decrease in the signal of the PAN compound, and by the TRENI,



312 which monitored the concentrations of NO and NO₂. The PAN dissociation reaction is a
 313 reversible process, where the dissociation products, peroxyacyl (PA) radical and NO₂, can re-
 314 combine to form PAN. With the addition of the large amount of NO, PA radicals are
 315 predominantly consumed by the irreversible PA + NO reaction, leading to the decay of the PAN
 316 compound. The apparent PAN dissociation rate constant can be described by Eq. 6 (Shepson et
 317 al., 1992), where k is the first-order loss rate constant measured by the CIMS (Fig. S6), k_{PAN} is
 318 the real PAN dissociation rate constant, $[NO]$ and $[NO_2]$ are the concentrations for NO and NO₂,
 319 and k_{NO} and k_{NO_2} are the rate constants for PA + NO and PA + NO₂ reactions. Since the rate
 320 constants k_{NO} and k_{NO_2} for the carbonyl nitrate-derived PA radical are unknown, the IUPAC
 321 recommended rate constants for the peroxyacetyl radicals (CH₃C(O)O₂) are used, with $k_{NO} =$
 322 $2.0 \times 10^{-11} \text{ cm}^3 \text{ molecule}^{-1} \text{ s}^{-1}$ and $k_{NO_2} = 8.9 \times 10^{-12} \text{ cm}^3 \text{ molecule}^{-1} \text{ s}^{-1}$. The PAN dissociation
 323 rate constant, after correcting for the competing PA + NO and PA + NO₂ reactions using Eq. 6, is
 324 $5.7(\pm 0.8) \times 10^{-4} \text{ s}^{-1}$, based on three experimental trials. In addition to dissociation, the PAN
 325 compound in the 100 L bag could also undergo wall loss. This loss rate was estimated by
 326 multiplying the wall loss rate of the carbonyl nitrate in the 5500 L chamber by a factor of 16,
 327 which is the square diffusion distance of the chamber relative to that of the 100 L bag, assuming
 328 the PAN compound and the isoprene carbonyl nitrate have similar diffusion and adsorption
 329 coefficients. Considering the uncertainty in wall loss rate, the PAN dissociation rate constant is
 330 $5.7(+0.8/-2.8) \times 10^{-4} \text{ s}^{-1}$. Previous studies of the dissociation rate constants for peroxyacyl nitrates
 331 have reported results ranging from $1.6 \times 10^{-4} \text{ s}^{-1}$ to $6.0 \times 10^{-4} \text{ s}^{-1}$ at 298 K (Bridier et al., 1991;
 332 Grosjean et al., 1994; Kabir et al., 2014; Roberts and Bertman, 1992). Our result is consistent
 333 with previous work.

$$334 \quad k = k_{PAN} \left(1 - \frac{1}{1 + \frac{k_{NO}[NO]}{k_{NO_2}[NO_2]}} \right) \quad (\text{Eq. 6})$$

335 Since our OH oxidation experiments were conducted in the presence of high NO concentration, a
 336 significant fraction of the PA radicals from the H abstraction reaction channel were expected to
 337 react with NO to form alkoxy radicals. Based on the product observed at m/z 321, a reaction
 338 scheme (Fig. 11) is proposed, where the alkoxy radical dissociates into CO₂ and an alkyl radical,
 339 which is further oxidized to form a C4 dinitrate (m/z 321, Fig. 10), along with ethanal nitrate
 340 (m/z 232, Fig. 10).



341 For the OH addition pathway, OH can add to the C2 and the C3 position of the 4,1-isoprene
342 carbonyl nitrate, but the less substituted C3 position should be preferential (Peeters et al., 2007).
343 For the C2 addition, the expected nitrate products are C5 dinitrate and ethanal nitrate (Fig. 12a),
344 as observed at m/z 351 and m/z 232 (Fig. 10). NO_2 could potentially be released with the
345 concurrent formation of a C4 di-aldehyde (Fig. 12a). The CIMS signal for this compound at m/z
346 229 did not increase (Fig. 10), but the CIMS sensitivity for this compound could be relatively
347 low. For the C3 addition, the expected nitrate products are C5 dinitrate, MVK nitrate and ethanal
348 nitrate (Fig. 12b), observed at m/z 351, m/z 276 and m/z 232 (Fig. 10). The C2 and C3 OH
349 addition pathway would lead to two C5 dinitrate isomers, but they were detected at the same
350 mass by the CIMS.

351 Using a GC-ECD/CIMS method similar to the one described by Xiong et al. (2015), the CIMS
352 sensitivities of the nitrate products were determined relative to the CIMS sensitivity of the 4,1-
353 carbonyl nitrate. The setup was modified to operate the GC separation under pressure lower than
354 1 atm (Fig. S7), which helped to lower the elution temperature. A Teflon bag filled with the 4,1-
355 carbonyl nitrate, isopropyl nitrite, and NO was irradiated to generate the OH oxidation products.
356 The mixture of the 4,1-carbonyl nitrate and its products were then cryo-focused and separated on
357 the GC column, and eluent species were detected by the ECD and the CIMS simultaneously. We
358 were able to quantify the MVK nitrate and the ethanal nitrate using this method, assuming
359 identical ECD sensitivities for nitrates. The other products shown in Fig. 10, however, were not
360 detected with simultaneous good signal-to-noise ratio on the ECD and the CIMS. The
361 ECD/CIMS chromatograms are shown in Fig. 13. We determined that the reaction of the 4,1-
362 carbonyl nitrate and the reagent ion I^- could form NO_3^- , but the same reaction did not occur for
363 the MVK nitrate and the ethanal nitrate (Fig. 13). Formation of NO_3^- from I^- reaction with
364 organic nitrates has not been reported previously. Since I^- is a poor nucleophile, it is unclear if
365 this reaction proceeds by $\text{S}_{\text{N}}2$ substitution. Using the same I^- ionization method, Wang et al.
366 (2014) observed NO_3^- signal equivalent to a $\text{NO}_3 + \text{N}_2\text{O}_5$ concentration of 200-1000 ppt during a
367 field study in Hong Kong. Through interference tests, the authors attributed 30-50% of the
368 observed NO_3^- signal to the interference from peroxyacetyl nitrate and NO_2 . Since I^- reaction
369 with the carbonyl nitrate can also generate NO_3^- , organic nitrates (RONO_2) could be a potential
370 source of interference for $\text{NO}_3 + \text{N}_2\text{O}_5$ measurement with the I^- ionization method.



371 For the GC-ECD/CIMS calibration, 9 trials were conducted at three different pressures. The
372 results are summarized in Table S2. The relative CIMS sensitivities for the 4,1-carbonyl nitrate,
373 ethanal nitrate and MVK nitrate are 1:15(±3):34(±3) respectively. The absolute CIMS sensitivity
374 of the 4,1-carbonyl nitrate was determined with standard gas samples prepared following Xiong
375 et al. (2015), and the result was used to calculate the absolute sensitivities for the ethanal nitrate
376 and the MVK nitrate. The ethanal nitrate and the MVK nitrate both have the $-\text{ONO}_2$ group at the
377 β position of the acidic H, so their CIMS sensitivities are comparable. For the MVK nitrate, the
378 electron-withdrawing ketone group can further enhance its gas-phase acidity and its affinity to
379 bind with I. Hence, the CIMS sensitivity for the MVK nitrate is greater than for the ethanal
380 nitrate. For the 4,1-carbonyl nitrate, its low CIMS sensitivity can be caused by the *trans*- δ
381 configuration of the $-\text{ONO}_2$ group and the $-\text{CHO}$ group. Our previous studies on isoprene-
382 derived hydroxynitrates suggested that the CIMS sensitivity for the β isomer is 8 times greater
383 than for the *trans*- δ isomer (Xiong et al., 2015). Lee et al. (2014a) also reported the β isomer
384 sensitivity being over 16 times greater than the *trans*- δ isomer sensitivity, using iodide as the
385 reagent ion. Hence, our calibration results, with the sensitivity for the ethanal nitrate 15 times
386 greater than the sensitivity for the 4,1-carbonyl nitrate, is consistent with previous work.

387 With the CIMS sensitivities determined, the yield of the MVK nitrate and the ethanal nitrate
388 from the OH-initiated oxidation of 4,1-carbonyl nitrate was obtained by comparing the formation
389 of the products relative to the loss of the reactant (Fig. 14). The ethanal nitrate was corrected for
390 loss to OH oxidation and photolysis, using the method described by Tuazon et al. (1984). The
391 applied ethanal nitrate + OH rate constant was $3.4 \times 10^{-12} \text{ cm}^3 \text{ molecules}^{-1} \text{ s}^{-1}$, calculated using the
392 structure-reactivity relationship proposed by Kwok and Atkinson (1995). The photolysis
393 frequency of the isoprene carbonyl nitrate was applied to account for the photolytic loss of
394 ethanal nitrate inside the chamber, because the β -ketone group is known to enhance the
395 absorption cross section of the nitrate (Müller et al., 2014). For the MVK nitrate, no OH loss
396 correction was applied, because MVK nitrate is saturated and is not expected to undergo
397 significant loss to OH. However, its loss to wall uptake and photolysis loss was corrected,
398 following the same method as used for the ethanal nitrate. The MVK nitrate loss rates for wall
399 uptake and photolysis inside the chamber were set the same as those for the 4,1-carbonyl nitrate,
400 because MVK nitrate is also a ketone nitrate, which is prone to photolysis loss, and it has a
401 molecular weight close to that of the 4,1-carbonyl nitrate. The apparent yield is 24.5% for MVK



402 nitrate and 8.08% for ethanal nitrate. Considering the uncertainties in the sensitivities of MVK
403 nitrate and ethanal nitrate (Table S2), the MVK nitrate yield is 24(±3)%, and the ethanal nitrate
404 yield is 8(±2)%. The fractional inlet sampling loss for the three nitrates was determined by
405 comparing the CIMS signals of sampling through the 5.2 m long 50°C tubing and through a 20
406 cm room temperature tubing. By correcting for the inlet sampling loss, the MVK nitrate yield is
407 24(±5)%, and the ethanal nitrate yield is 8(±3)%. For the two OH oxidation experiments, the
408 first-order loss rate of the 4,1-carbonyl nitrate was $3 \times 10^{-4} \text{ s}^{-1}$ (Fig. S8). Since the total wall
409 uptake and photolysis loss rate for 4,1-isoprene carbonyl nitrate was $4.3 \times 10^{-5} \text{ s}^{-1}$,
410 approximately 85% of the 4,1-carbonyl nitrate was lost to OH oxidation. After correcting for this
411 factor, the MVK nitrate yield is 28(±5)%, and the ethanal nitrate yield is 9(±3)%.

412 **4.3.2 Photolysis**

413 Previous work on acetaldehyde suggests that at 313 nm the dominant photolysis reaction is
414 dissociation of the C–CHO bond, forming a formyl radical ($\bullet\text{CHO}$) (Blacet and Loeffler, 1942).
415 At shorter wavelength (265 nm), the reaction can proceed by intramolecular rearrangement
416 forming CH_4 and CO (Blacet and Loeffler, 1942). For compounds with longer carbon chain
417 length, such as propyl- and butyl- aldehydes, the photo-dissociation reaction can produce alkenes
418 and smaller aldehydes at 238 nm and 187 nm (Blacet and Crane, 1954). Since the UV radiation
419 that reaches the earth's surface is mostly above 300 nm, the formyl radical pathway is expected
420 to be the most important photolysis reaction for alkyl aldehydes (Shepson and Heicklen, 1982).
421 For the isoprene carbonyl nitrate, the C–CHO bond is strengthened by the delocalized electrons
422 from the vinyl and the carbonyl groups, leading to a bond dissociation energy of 413 kJ/mol, as
423 measured for acrolein, which is larger than the C–CHO bond dissociation energy of acetaldehyde
424 (355 kJ/mol) (Wiberg et al., 1992). In comparison, the O–NO₂ bond dissociation energy is 175
425 kJ/mol (Luo, 2007b), much lower than the dissociation energy of the C–CHO bond. Hence,
426 dissociation of the weak O–NO₂ bond may be an important reaction pathway for the carbonyl
427 nitrate. This process likely involves the absorption of a photon by the C=C–C=O chromophore,
428 followed by intramolecular energy redistribution to deposit energy into the O–NO₂ bond prior to
429 dissociation. This reaction step would generate NO₂ and an alkoxy radical, which upon reaction
430 with O₂ forms a conjugated dialdehyde.



431 Fig. 15 shows the CIMS spectra before and after the photolysis of the isoprene carbonyl nitrate.
432 Cyclohexane was used as the OH scavenger for this experiment. The CIMS signal for the
433 dialdehyde, which is the O–NO₂ bond dissociation product (reaction mechanism shown in Fig.
434 16), did not increase significantly. This may be because the CIMS was not sensitive to the
435 dialdehyde, and/or the dialdehyde underwent rapid secondary reactions, rendering its steady-state
436 concentration below the CIMS detection limit. Alternatively, it is possible that the alkoxy radical
437 derived from O–NO₂ bond dissociation undergoes a 1,5-H shift reaction (Fig. 16), rendering the
438 formation of the dialdehyde an insignificant pathway. The resulting alkyl radical can
439 immediately form a peroxy radical, which may follow the H shift mechanism proposed by
440 Peeters et al. (2009) and form a hydroperoxy aldehyde (HPALD) compound, as observed at m/z
441 257 by the CIMS (Fig. 15). When the peroxy radical reacts with NO or RO₂, the resulting alkoxy
442 radical will form a hydroxy dialdehyde (Fig. 16) with m/z ratio at 241, which was also observed
443 by the CIMS (Fig. 14). It is worth noting that we also observed CIMS signals for the
444 deprotonated ions derived from the HPALD compound (m/z 129 and m/z 147) and the hydroxy
445 dialdehyde (m/z 113 and m/z 131). The proton transfer reaction between the iodide ion and
446 alcohols/peroxides have not been observed previously, but it is possible that the conjugated
447 structures help stabilize the charge and hence make the proton transfer reaction a viable reaction
448 channel.

449 The product at m/z 276 has the molecular weight of MVK nitrate. In the presence of OH
450 scavenger, however, the reaction is unlikely to proceed by the OH-initiated oxidation pathway to
451 form MVK nitrate. Instead, we hypothesize that the isoprene carbonyl nitrate could dissociate via
452 the C–CHO bond, which, following reaction with O₂ and HO₂, would form a vinyl
453 hydroperoxide with the same molecular weight as MVK nitrate. Vinyl hydroperoxides are
454 known to be a reactive intermediate from the intramolecular H shift of Criegee biradical, which
455 can decompose into OH and alkoxy radicals (Kroll et al., 2002). However, the un-energized
456 vinyl hydroperoxides should have a lifetime long enough to be detected by mass spectrometers
457 (Liu et al., 2015). In fact, theoretical calculations suggest that at 25 °C vinyl hydroperoxide has a
458 lifetime of 58 hours (Richardson, 1995). Therefore, the product at m/z 276 is likely the vinyl
459 hydroperoxide. For the OH oxidation product experiments, however, we attributed m/z 276 to
460 MVK nitrate only, because RO₂ + NO reaction (forming MVK nitrate) should dominate over
461 RO₂ + HO₂ reaction (forming vinyl hydroperoxide), in the presence of high NO concentration.



462 Based on the CIMS spectra of the photolysis products, we conclude that the photolysis of the
463 isoprene carbonyl nitrate leads to the dissociation of both the O–NO₂ and the C–CHO bonds. A
464 reaction scheme is proposed in Fig. 16. Future studies are needed to evaluate the relative
465 importance of these two processes.

466 5 Conclusions and future work

467 An isoprene-derived carbonyl nitrate model compound was synthesized to study its
468 photochemical degradation chemistry in the atmosphere. The UV absorption spectrum of this
469 compound has contributions from both the C=C–C=O and the –ONO₂ chromophores, as is
470 confirmed by theoretical calculations, but absorption in the actinic region involves a transition
471 involving the carbonyl group. The combination of the C=C–C=O and the –ONO₂ chromophores
472 enhances the UV cross section of this molecule relative to alkyl nitrates, making photolysis its
473 dominant daytime sink. The photochemical lifetime of the carbonyl nitrate can be less than one
474 hour, due to its rapid photolysis loss, together with high reactivity toward OH and O₃. The OH
475 and O₃ oxidation rate constants for the 4,1-isoprene carbonyl nitrate obtained in this study were
476 both smaller than the reported rate constants for the δ -isoprene hydroxy nitrates (Jacobs et al.,
477 2014; Lee et al., 2014b). This could be because the oxidation by either OH or O₃ would break the
478 resonance structure of the C=C–C=O moiety, thus increasing the activation energy.

479 Using the iodide-based CIMS, we identified the first-generation nitrate products from the OH-
480 initiated oxidation of the synthesized carbonyl nitrate, including mononitrate, dinitrate and
481 nitrooxy peroxyacyl nitrate. Two of the products, the MVK nitrate and the ethanal nitrate, were
482 quantified, which contributed to 37(±5)% of the total products. The CIMS spectra of the nitrate
483 photolysis products suggest that both the C–CHO bond and the O–NO₂ bond dissociate in the
484 reaction. Since photolysis is a significant sink for the carbonyl nitrate, it is important for future
485 studies to investigate the relative importance of the two reaction pathways, in order to fully
486 understand the fate of NO_x in isoprene-rich atmospheres. Dissociation of the O–NO₂ bond may
487 afford highly oxidized alcohol and hydroperoxide, which can potentially undergo uptake into the
488 particle phase and facilitate the formation of secondary organic aerosols. The C–CHO
489 dissociation pathway may form a vinyl hydroperoxide product.



490 The NO₃-initiated isoprene oxidation can produce a series of carbonyl nitrates. The 1,4-carbonyl
491 nitrate, which is the dominant isomer, is expected to have similar photolysis reactivity as the 4,1-
492 carbonyl nitrate studied in this work, because they both have the O=C–C=C–C chromophore and
493 the –ONO₂ chromophore, which would enhance the molecular absorption cross section. The
494 influence of the unsaturated ketone functionality on nitrate photolysis is still unclear, and future
495 studies are needed to understand how the different conjugated structures can affect the
496 photochemical processes.

497 The experiments in this work were conducted in the presence of relatively high NO
498 concentration. In the ambient environment, organic nitrates produced in the high NO_x regime can
499 undergo photochemical degradation in the low NO regime, due to the wide span of ambient NO_x
500 concentrations (Su et al., 2015; Xiong et al., 2015). Crouse et al. (2012) proposed that under
501 low NO conditions, the oxidation of methacrolein (MACR) can regenerate OH radicals and form
502 a lactone that is prone to reactive uptake onto the aerosol phase. Since the 4,1-carbonyl nitrate
503 has a structure similar to that of MACR, it might also undergo similar reaction in the clean
504 environment. Further experimental work is needed to investigate how the photochemical
505 oxidation process of the carbonyl nitrate can influence the formation of OH radicals and growth
506 of secondary organic aerosols.

507 **Acknowledgement**

508 This research was supported in part through computational resources provided by Information
509 Technology at Purdue University. We thank the National Science Foundation for supporting
510 CHB and LVS (grant CHE-1465154), and FX and PBS (grant AGS-1228496).

511 **References**

512 Aschmann, S. M., Tuazon, E. C., Arey, J., and Atkinson, R.: Products of the OH radical-initiated
513 reactions of 2-propyl nitrate, 3-methyl-2-butyl nitrate and 3-methyl-2-pentyl nitrate,
514 Atmospheric Environment, 45, 1695-1701, <http://dx.doi.org/10.1016/j.atmosenv.2010.12.061>,
515 2011.

516 Atkinson, R., and Aschmann, S. M.: Kinetics of the gas phase reaction of Cl atoms with a series
517 of organics at 296 ± 2 K and atmospheric pressure, International Journal of Chemical Kinetics,
518 17, 33-41, 10.1002/kin.550170105, 1985.



- 519 Atkinson, R., Baulch, D. L., Cox, R. A., Crowley, J. N., Hampson, R. F., Hynes, R. G., Jenkin, M. E.,
520 Rossi, M. J., and Troe, J.: Evaluated kinetic and photochemical data for atmospheric chemistry:
521 Volume III – gas phase reactions of inorganic halogens, *Atmos. Chem. Phys.*, 7, 981-1191,
522 10.5194/acp-7-981-2007, 2007.
- 523 Bayliss, N. S., and McRae, E. G.: Solvent Effects in the Spectra of Acetone, Crotonaldehyde,
524 Nitromethane and Nitrobenzene, *The Journal of Physical Chemistry*, 58, 1006-1011,
525 10.1021/j150521a018, 1954.
- 526 Blacet, F. E., and Loeffler, D. E.: The Photolysis of the Aliphatic Aldehydes. XI. Acetaldehyde and
527 Iodine Mixtures, *Journal of the American Chemical Society*, 64, 893-896, 10.1021/ja01256a045,
528 1942.
- 529 Blacet, F. E.: Photochemistry in the Lower Atmosphere, *Industrial & Engineering Chemistry*, 44,
530 1339-1342, 10.1021/ie50510a044, 1952.
- 531 Blacet, F. E., and Crane, R. A.: The Photolysis of the Aliphatic Aldehydes. XVII. Propionaldehyde,
532 n-Butyraldehyde and Isobutyraldehyde at 2380 and 1870 Å, *Journal of the American Chemical*
533 *Society*, 76, 5337-5340, 10.1021/ja01650a020, 1954.
- 534 Braun, W., Fahr, A., Klein, R., Kurylo, M. J., and Huie, R. E.: UV gas and liquid phase absorption
535 cross section measurements of hydrochlorofluorocarbons HCFC-225ca and HCFC-225cb, *Journal*
536 *of Geophysical Research: Atmospheres*, 96, 13009-13015, 10.1029/91JD01026, 1991.
- 537 Bridier, I., Caralp, F., Loirat, H., Lesclaux, R., Veyret, B., Becker, K. H., Reimer, A., and Zabel, F.:
538 Kinetic and theoretical studies of the reactions acetylperoxy + nitrogen dioxide + M .dblarw.
539 acetyl peroxy + M between 248 and 393 K and between 30 and 760 torr, *The Journal of*
540 *Physical Chemistry*, 95, 3594-3600, 10.1021/j100162a031, 1991.
- 541 Brown, S. S., deGouw, J. A., Warneke, C., Ryerson, T. B., Dubé, W. P., Atlas, E., Weber, R. J.,
542 Peltier, R. E., Neuman, J. A., Roberts, J. M., Swanson, A., Flocke, F., McKeen, S. A., Brioude, J.,
543 Sommariva, R., Trainer, M., Fehsenfeld, F. C., and Ravishankara, A. R.: Nocturnal isoprene
544 oxidation over the Northeast United States in summer and its impact on reactive nitrogen
545 partitioning and secondary organic aerosol, *Atmos. Chem. Phys.*, 9, 3027-3042, 10.5194/acp-9-
546 3027-2009, 2009.
- 547 Chai, J.-D., and Head-Gordon, M.: Long-range corrected hybrid density functionals with damped
548 atom-atom dispersion corrections, *Physical Chemistry Chemical Physics*, 10, 6615-6620,
549 10.1039/B810189B, 2008.
- 550 Chameides, W., and Walker, J. C. G.: A photochemical theory of tropospheric ozone, *Journal of*
551 *Geophysical Research*, 78, 8751-8760, 10.1029/JC078i036p08751, 1973.
- 552 Chameides, W., Lindsay, R., Richardson, J., and Kiang, C.: The role of biogenic hydrocarbons in
553 urban photochemical smog: Atlanta as a case study, *Science*, 241, 1473-1475,
554 10.1126/science.3420404, 1988.



- 555 Chameides, W. L., Fehsenfeld, F., Rodgers, M. O., Cardelino, C., Martinez, J., Parrish, D.,
556 Lonneman, W., Lawson, D. R., Rasmussen, R. A., Zimmerman, P., Greenberg, J., Middleton, P.,
557 and Wang, T.: Ozone precursor relationships in the ambient atmosphere, *Journal of*
558 *Geophysical Research: Atmospheres*, 97, 6037-6055, 10.1029/91JD03014, 1992.
- 559 Chen, X., Hulbert, D., and Shepson, P. B.: Measurement of the organic nitrate yield from OH
560 reaction with isoprene, *Journal of Geophysical Research*, 103, 25563, 10.1029/98jd01483, 1998.
- 561 Crouse, J. D., Knap, H. C., Oronso, K. B., Jorgensen, S., Paulot, F., Kjaergaard, H. G., and
562 Wennberg, P. O.: Atmospheric fate of methacrolein. 1. Peroxy radical isomerization following
563 addition of OH and O₂, *The journal of physical chemistry. A*, 116, 5756-5762,
564 10.1021/jp211560u, 2012.
- 565 Darer, A. I., Cole-Filipiak, N. C., O'Connor, A. E., and Elrod, M. J.: Formation and stability of
566 atmospherically relevant isoprene-derived organosulfates and organonitrates, *Environmental*
567 *science & technology*, 45, 1895-1902, 10.1021/es103797z, 2011.
- 568 Ferris, A. F., McLean, K. W., Marks, I. G., and Emmons, W. D.: Metathetical Reactions of Silver
569 Salts in Solution. III. The Synthesis of Nitrate Esters¹, *Journal of the American Chemical Society*,
570 75, 4078-4078, 10.1021/ja01112a505, 1953.
- 571 Frisch, M. J., Pople, J. A., and Binkley, J. S.: Self - consistent molecular orbital methods 25.
572 Supplementary functions for Gaussian basis sets, *The Journal of Chemical Physics*, 80, 3265-
573 3269, doi:<http://dx.doi.org/10.1063/1.447079>, 1984.
- 574 Giacomelli, P., Ford, K., Espada, C., and Shepson, P. B.: Comparison of the measured and
575 simulated isoprene nitrate distributions above a forest canopy, *Journal of Geophysical Research*,
576 110, D01304, 10.1029/2004jd005123, 2005.
- 577 Gilbert, A. T. B.: IQmol molecular viewer, 2012.
- 578 Gray, G. M.: Method for the preparation of (E)-4-bromo-2-methylbut-2-en-1-al 4288635, 1981.
- 579 Grosjean, D., Grosjean, E., and Williams, E. L.: Thermal decomposition of C₃-substituted
580 peroxyacyl nitrates, *Res Chem Intermed*, 20, 447-461, 10.1163/156856794X00414, 1994.
- 581 Grossenbacher, J. W., Barket Jr, D. J., Shepson, P. B., Carroll, M. A., Olszyna, K., and Apel, E.: A
582 comparison of isoprene nitrate concentrations at two forest-impacted sites, *Journal of*
583 *Geophysical Research: Atmospheres*, 109, D11311, 10.1029/2003JD003966, 2004.
- 584 Haagen-Smit, A. J.: Chemistry and Physiology of Los Angeles Smog, *Industrial & Engineering*
585 *Chemistry*, 44, 1342-1346, 10.1021/ie50510a045, 1952.
- 586 Hallquist, M., Wängberg, I., and Ljungström, E.: Atmospheric Fate of Carbonyl Oxidation
587 Products Originating from α -Pinene and Δ^3 -Carene: Determination of Rate of Reaction with OH



- 588 and NO₃ Radicals, UV Absorption Cross Sections, and Vapor Pressures, *Environmental science &*
589 *technology*, 31, 3166-3172, 10.1021/es970151a, 1997.
- 590 Herron, J. T., and Huie, R. E.: Rate constants for the reactions of ozone with ethene and
591 propene, from 235.0 to 362.0.deg.K, *The Journal of Physical Chemistry*, 78, 2085-2088,
592 10.1021/j100614a004, 1974.
- 593 Hohenberg, P., and Kohn, W.: Inhomogeneous Electron Gas, *Physical Review*, 136, B864-B871,
594 1964.
- 595 Horowitz, L. W., Fiore, A. M., Milly, G. P., Cohen, R. C., Perring, A., Wooldridge, P. J., Hess, P. G.,
596 Emmons, L. K., and Lamarque, J.-F.: Observational constraints on the chemistry of isoprene
597 nitrates over the eastern United States, *Journal of Geophysical Research*, 112, D12S08,
598 10.1029/2006jd007747, 2007.
- 599 Hu, K. S., Darer, A. I., and Elrod, M. J.: Thermodynamics and kinetics of the hydrolysis of
600 atmospherically relevant organonitrates and organosulfates, *Atmospheric Chemistry and*
601 *Physics*, 11, 8307-8320, 10.5194/acp-11-8307-2011, 2011.
- 602 Jacobs, M. I., Burke, W. J., and Elrod, M. J.: Kinetics of the reactions of isoprene-derived
603 hydroxynitrates: gas phase epoxide formation and solution phase hydrolysis, *Atmospheric*
604 *Chemistry and Physics*, 14, 8933-8946, 10.5194/acp-14-8933-2014, 2014.
- 605 Kabir, M., Jagiella, S., and Zabel, F.: Thermal Stability of n-Acyl Peroxynitrates, *International*
606 *Journal of Chemical Kinetics*, 46, 462-469, 10.1002/kin.20862, 2014.
- 607 Klein, T., Barnes, I., Becker, K. H., Fink, E. H., and Zabel, F.: Pressure dependence of the rate
608 constants for the reactions of ethene and propene with hydroxyl radicals at 295 K, *The Journal*
609 *of Physical Chemistry*, 88, 5020-5025, 10.1021/j150665a046, 1984.
- 610 Kohn, W., and Sham, L. J.: Self-Consistent Equations Including Exchange and Correlation Effects,
611 *Physical Review*, 140, A1133-A1138, 1965.
- 612 Kroll, J. H., Donahue, N. M., Cee, V. J., Demerjian, K. L., and Anderson, J. G.: Gas-Phase
613 Ozonolysis of Alkenes: Formation of OH from Anti Carbonyl Oxides, *Journal of the American*
614 *Chemical Society*, 124, 8518-8519, 10.1021/ja0266060, 2002.
- 615 Kwan, A. J., Chan, A. W. H., Ng, N. L., Kjaergaard, H. G., Seinfeld, J. H., and Wennberg, P. O.:
616 Peroxy radical chemistry and OH radical production during the NO₃-initiated
617 oxidation of isoprene, *Atmospheric Chemistry and Physics*, 12, 7499-7515, 10.5194/acp-12-
618 7499-2012, 2012.
- 619 Kwok, E. S. C., and Atkinson, R.: Estimation of hydroxyl radical reaction rate constants for gas-
620 phase organic compounds using a structure-reactivity relationship: An update, *Atmospheric*
621 *Environment*, 29, 1685-1695, [http://dx.doi.org/10.1016/1352-2310\(95\)00069-B](http://dx.doi.org/10.1016/1352-2310(95)00069-B), 1995.



- 622 Lee, B. H., Lopez-Hilfiker, F. D., Mohr, C., Kurtén, T., Worsnop, D. R., and Thornton, J. A.: An
623 Iodide-Adduct High-Resolution Time-of-Flight Chemical-Ionization Mass Spectrometer:
624 Application to Atmospheric Inorganic and Organic Compounds, *Environmental science &*
625 *technology*, 48, 6309-6317, 10.1021/es500362a, 2014a.
- 626 Lee, L., Teng, A. P., Wennberg, P. O., Crouse, J. D., and Cohen, R. C.: On rates and mechanisms
627 of OH and O₃ reactions with isoprene-derived hydroxy nitrates, *The journal of physical*
628 *chemistry. A*, 118, 1622-1637, 10.1021/jp4107603, 2014b.
- 629 Lefohn, A. S., and Foley, J. K.: Establishing Relevant Ozone Standards to Protect Vegetation and
630 Human Health: Exposure/Dose-Response Considerations, *Air & Waste*, 43, 106-112,
631 10.1080/1073161X.1993.10467111, 1993.
- 632 Linder, B., and Abdunur, S.: Solvent Effects on Electronic Spectral Intensities, *The Journal of*
633 *Chemical Physics*, 54, 1807-1814, doi:<http://dx.doi.org/10.1063/1.1675088>, 1971.
- 634 Lippmann, M.: HEALTH EFFECTS OF OZONE A Critical Review, *JAPCA*, 39, 672-695,
635 10.1080/08940630.1989.10466554, 1989.
- 636 Liu, F., Fang, Y., Kumar, M., Thompson, W. H., and Lester, M. I.: Direct observation of vinyl
637 hydroperoxide, *Physical Chemistry Chemical Physics*, 17, 20490-20494, 10.1039/C5CP02917A,
638 2015.
- 639 Lockwood, A. L., Shepson, P. B., Fiddler, M. N., and Alaghmand, M.: Isoprene nitrates:
640 preparation, separation, identification, yields, and atmospheric chemistry, *Atmospheric*
641 *Chemistry and Physics*, 10, 6169-6178, 10.5194/acp-10-6169-2010, 2010.
- 642 Lu, K. D., Rohrer, F., Holland, F., Fuchs, H., Bohn, B., Brauers, T., Chang, C. C., Häseler, R., Hu, M.,
643 Kita, K., Kondo, Y., Li, X., Lou, S. R., Nehr, S., Shao, M., Zeng, L. M., Wahner, A., Zhang, Y. H., and
644 Hofzumahaus, A.: Observation and modelling of OH and HO₂ concentrations in the Pearl River
645 Delta 2006: a missing OH source in a VOC rich atmosphere, *Atmos. Chem. Phys.*, 12, 1541-1569,
646 10.5194/acp-12-1541-2012, 2012.
- 647 Luo, Y.-R.: BDEs in the halogenated molecules, clusters and complexes, in: *Comprehensive*
648 *Handbook of Chemical Bond Energies*, CRC Press, 1351-1427, 2007a.
- 649 Luo, Y.-R.: BDEs of O-X bonds, in: *Comprehensive Handbook of Chemical Bond Energies*, CRC
650 Press, 351, 2007b.
- 651 Madronich, S., and Flocke, S.: The role of solar radiation in atmospheric chemistry, in:
652 *Handbook of Environmental Chemistry*, edited by: Boule, P., Springer-Verlag, Heidelberg, 1-26,
653 1998.
- 654 Mao, J., Paulot, F., Jacob, D. J., Cohen, R. C., Crouse, J. D., Wennberg, P. O., Keller, C. A.,
655 Hudman, R. C., Barkley, M. P., and Horowitz, L. W.: Ozone and organic nitrates over the eastern



- 656 United States: Sensitivity to isoprene chemistry, *Journal of Geophysical Research: Atmospheres*,
657 118, 11,256-211,268, 10.1002/jgrd.50817, 2013.
- 658 Martinez, M., Harder, H., Kovacs, T. A., Simpas, J. B., Bassis, J., Leshner, R., Brune, W. H., Frost, G.
659 J., Williams, E. J., Stroud, C. A., Jobson, B. T., Roberts, J. M., Hall, S. R., Shetter, R. E., Wert, B.,
660 Fried, A., Alicke, B., Stutz, J., Young, V. L., White, A. B., and Zamora, R. J.: OH and HO₂
661 concentrations, sources, and loss rates during the Southern Oxidants Study in Nashville,
662 Tennessee, summer 1999, *Journal of Geophysical Research: Atmospheres*, 108, n/a-n/a,
663 10.1029/2003JD003551, 2003.
- 664 Mihelcic, D., Holland, F., Hofzumahaus, A., Hoppe, L., Konrad, S., Müsgen, P., Pätz, H. W.,
665 Schäfer, H. J., Schmitz, T., Volz-Thomas, A., Bächmann, K., Schlomski, S., Platt, U., Geyer, A.,
666 Alicke, B., and Moortgat, G. K.: Peroxy radicals during BERLIOZ at Pabstthum: Measurements,
667 radical budgets and ozone production, *Journal of Geophysical Research: Atmospheres*, 108,
668 n/a-n/a, 10.1029/2001JD001014, 2003.
- 669 Müller, J. F., Peeters, J., and Stavrou, T.: Fast photolysis of carbonyl nitrates from isoprene,
670 *Atmospheric Chemistry and Physics*, 14, 2497-2508, 10.5194/acp-14-2497-2014, 2014.
- 671 Neuman, J. A., Nowak, J. B., Huey, L. G., Burkholder, J. B., Dibb, J. E., Holloway, J. S., Liao, J.,
672 Peischl, J., Roberts, J. M., Ryerson, T. B., Scheuer, E., Stark, H., Stickel, R. E., Tanner, D. J., and
673 Weinheimer, A.: Bromine measurements in ozone depleted air over the Arctic Ocean, *Atmos.*
674 *Chem. Phys.*, 10, 6503-6514, 10.5194/acp-10-6503-2010, 2010.
- 675 Noyes, W. A.: Explanation of the Formation of Alkyl Nitrites in Dilute Solutions; Butyl and Amyl
676 Nitrites, *Journal of the American Chemical Society*, 55, 3888-3889, 10.1021/ja01336a503, 1933.
- 677 Parrish, D. D., Lamarque, J. F., Naik, V., Horowitz, L., Shindell, D. T., Staehelin, J., Derwent, R.,
678 Cooper, O. R., Tanimoto, H., Volz-Thomas, A., Gilge, S., Scheel, H. E., Steinbacher, M., and
679 Fröhlich, M.: Long-term changes in lower tropospheric baseline ozone concentrations:
680 Comparing chemistry-climate models and observations at northern midlatitudes, *Journal of*
681 *Geophysical Research: Atmospheres*, 119, 5719-5736, 10.1002/2013JD021435, 2014.
- 682 Patchen, A. K., Pennino, M. J., Kiep, A. C., and Elrod, M. J.: Direct kinetics study of the product-
683 forming channels of the reaction of isoprene-derived hydroxyperoxy radicals with NO,
684 *International Journal of Chemical Kinetics*, 39, 353-361, 10.1002/kin.20248, 2007.
- 685 Paulot, F., Crouse, J. D., Kjaergaard, H. G., Kroll, J. H., Seinfeld, J. H., and Wennberg, P. O.:
686 Isoprene photooxidation: new insights into the production of acids and organic nitrates, *Atmos.*
687 *Chem. Phys.*, 9, 1479-1501, 10.5194/acp-9-1479-2009, 2009.
- 688 Paulot, F., Henze, D. K., and Wennberg, P. O.: Impact of the isoprene photochemical cascade on
689 tropical ozone, *Atmospheric Chemistry and Physics*, 12, 1307-1325, 10.5194/acp-12-1307-2012,
690 2012.



- 691 Peeters, J., Boullart, W., Pultau, V., Vandenberg, S., and Vereecken, L.: Structure–Activity
692 Relationship for the Addition of OH to (Poly)alkenes: Site-Specific and Total Rate Constants,
693 The Journal of Physical Chemistry A, 111, 1618-1631, 10.1021/jp066973o, 2007.
- 694 Peeters, J., Nguyen, T. L., and Vereecken, L.: HOx radical regeneration in the oxidation of
695 isoprene, Physical chemistry chemical physics : PCCP, 11, 5935-5939, 10.1039/b908511d, 2009.
- 696 Perring, A. E., Wisthaler, A., Graus, M., Wooldridge, P. J., Lockwood, A. L., Mielke, L. H., Shepson,
697 P. B., Hansel, A., and Cohen, R. C.: A product study of the isoprene+NO₃ reaction, Atmos. Chem.
698 Phys., 9, 4945-4956, 10.5194/acp-9-4945-2009, 2009.
- 699 Platt, U., Aliche, B., Dubois, R., Geyer, A., Hofzumahaus, A., Holland, F., Martinez, M., Mihelcic,
700 D., Klüpfel, T., Lohrmann, B., Pätz, W., Perner, D., Rohrer, F., Schäfer, J., and Stutz, J.: Free
701 Radicals and Fast Photochemistry during BERLIOZ, Journal of Atmospheric Chemistry, 42, 359-
702 394, 10.1023/A:1015707531660, 2002.
- 703 Richardson, W. H.: An Evaluation of Vinyl Hydroperoxide as an Isolable Molecule, The Journal of
704 Organic Chemistry, 60, 4090-4095, 10.1021/jo00118a027, 1995.
- 705 Rindelaub, J. D., McAvey, K. M., and Shepson, P. B.: The photochemical production of organic
706 nitrates from α -pinene and loss via acid-dependent particle phase hydrolysis, Atmospheric
707 Environment, 100, 193-201, <http://dx.doi.org/10.1016/j.atmosenv.2014.11.010>, 2015.
- 708 Roberts, J. M.: The atmospheric chemistry of organic nitrates, Atmospheric Environment. Part A.
709 General Topics, 24, 243-287, [http://dx.doi.org/10.1016/0960-1686\(90\)90108-Y](http://dx.doi.org/10.1016/0960-1686(90)90108-Y), 1990.
- 710 Roberts, J. M., and Bertman, S. B.: The thermal decomposition of peroxyacetic nitric anhydride
711 (PAN) and peroxyacrylic nitric anhydride (MPAN), International Journal of Chemical
712 Kinetics, 24, 297-307, 10.1002/kin.550240307, 1992.
- 713 Roberts, J. M., Flocke, F., Stroud, C. A., Hereid, D., Williams, E., Fehsenfeld, F., Brune, W.,
714 Martinez, M., and Harder, H.: Ground-based measurements of peroxyacetic nitric
715 anhydrides (PANs) during the 1999 Southern Oxidants Study Nashville Intensive, Journal of
716 Geophysical Research: Atmospheres, 107, ACH 1-1-ACH 1-10, 10.1029/2001JD000947, 2002.
- 717 Rollins, A. W., Kiendler-Scharr, A., Fry, J. L., Brauers, T., Brown, S. S., Dorn, H. P., Dubé, W. P.,
718 Fuchs, H., Mensah, A., Mentel, T. F., Rohrer, F., Tillmann, R., Wegener, R., Wooldridge, P. J., and
719 Cohen, R. C.: Isoprene oxidation by nitrate radical: alkyl nitrate and secondary organic aerosol
720 yields, Atmos. Chem. Phys., 9, 6685-6703, 10.5194/acp-9-6685-2009, 2009.
- 721 Runge, E., and Gross, E. K. U.: Density-Functional Theory for Time-Dependent Systems, Physical
722 Review Letters, 52, 997-1000, 1984.
- 723 Schwantes, R. H., Teng, A. P., Nguyen, T. B., Coggon, M. M., Crouse, J. D., St. Clair, J. M., Zhang,
724 X., Schilling, K. A., Seinfeld, J. H., and Wennberg, P. O.: Isoprene NO₃ Oxidation Products from
725 the RO₂ + HO₂ Pathway, The Journal of Physical Chemistry A, 10.1021/acs.jpca.5b06355, 2015.



- 726 Shao, Y., Gan, Z., Epifanovsky, E., Gilbert, A. T. B., Wormit, M., Kussmann, J., Lange, A. W., Behn,
727 A., Deng, J., Feng, X., Ghosh, D., Goldey, M., Horn, P. R., Jacobson, L. D., Kaliman, I., Khaliullin, R.
728 Z., Kuś, T., Landau, A., Liu, J., Proynov, E. I., Rhee, Y. M., Richard, R. M., Rohrdanz, M. A., Steele,
729 R. P., Sundstrom, E. J., Woodcock, H. L., Zimmerman, P. M., Zuev, D., Albrecht, B., Alguire, E.,
730 Austin, B., Beran, G. J. O., Bernard, Y. A., Berquist, E., Brandhorst, K., Bravaya, K. B., Brown, S. T.,
731 Casanova, D., Chang, C.-M., Chen, Y., Chien, S. H., Closser, K. D., Crittenden, D. L., Diedenhofen,
732 M., DiStasio, R. A., Do, H., Dutoi, A. D., Edgar, R. G., Fatehi, S., Fusti-Molnar, L., Ghysels, A.,
733 Golubeva-Zadorozhnaya, A., Gomes, J., Hanson-Heine, M. W. D., Harbach, P. H. P., Hauser, A.
734 W., Hohenstein, E. G., Holden, Z. C., Jagau, T.-C., Ji, H., Kaduk, B., Khistyayev, K., Kim, J., Kim, J.,
735 King, R. A., Klunzinger, P., Kosenkov, D., Kowalczyk, T., Krauter, C. M., Lao, K. U., Laurent, A. D.,
736 Lawler, K. V., Levchenko, S. V., Lin, C. Y., Liu, F., Livshits, E., Lochan, R. C., Luenser, A., Manohar,
737 P., Manzer, S. F., Mao, S.-P., Mardirossian, N., Marenich, A. V., Maurer, S. A., Mayhall, N. J.,
738 Neuscamman, E., Oana, C. M., Olivares-Amaya, R., O'Neill, D. P., Parkhill, J. A., Perrine, T. M.,
739 Peverati, R., Prociuk, A., Rehn, D. R., Rosta, E., Russ, N. J., Sharada, S. M., Sharma, S., Small, D.
740 W., Sodt, A., Stein, T., Stück, D., Su, Y.-C., Thom, A. J. W., Tsuchimochi, T., Vanovschi, V., Vogt, L.,
741 Vydrov, O., Wang, T., Watson, M. A., Wenzel, J., White, A., Williams, C. F., Yang, J., Yeganeh, S.,
742 Yost, S. R., You, Z.-Q., Zhang, I. Y., Zhang, X., Zhao, Y., Brooks, B. R., Chan, G. K. L., Chipman, D.
743 M., Cramer, C. J., Goddard, W. A., Gordon, M. S., Hehre, W. J., Klamt, A., Schaefer, H. F.,
744 Schmidt, M. W., Sherrill, C. D., Truhlar, D. G., Warshel, A., Xu, X., Aspuru-Guzik, A., Baer, R., Bell,
745 A. T., Besley, N. A., Chai, J.-D., Dreuw, A., Dunietz, B. D., Furlani, T. R., Gwaltney, S. R., Hsu, C.-P.,
746 Jung, Y., Kong, J., Lambrecht, D. S., Liang, W., Ochsenfeld, C., Rassolov, V. A., Slipchenko, L. V.,
747 Subotnik, J. E., Van Voorhis, T., Herbert, J. M., Krylov, A. I., Gill, P. M. W., and Head-Gordon, M.:
748 Advances in molecular quantum chemistry contained in the Q-Chem 4 program package,
749 Molecular Physics, 113, 184-215, 10.1080/00268976.2014.952696, 2015.
- 750 Shepson, P. B., and Heicklen, J.: The wavelength and pressure dependence of the photolysis of
751 propionaldehyde in air, Journal of Photochemistry, 19, 215-227,
752 [http://dx.doi.org/10.1016/0047-2670\(82\)80024-5](http://dx.doi.org/10.1016/0047-2670(82)80024-5), 1982.
- 753 Shepson, P. B., Bottenheim, J. W., Hastie, D. R., and Venkatram, A.: Determination of the
754 relative ozone and PAN deposition velocities at night, Geophysical Research Letters, 19, 1121-
755 1124, 10.1029/92GL01118, 1992.
- 756 Sprengnether, M., Demerjian, K. L., Donahue, N. M., and Anderson, J. G.: Product analysis of the
757 OH oxidation of isoprene and 1,3-butadiene in the presence of NO, Journal of Geophysical
758 Research, 107, 10.1029/2001jd000716, 2002.
- 759 Starn, T. K., Shepson, P. B., Bertman, S. B., Riemer, D. D., Zika, R. G., and Olszyna, K.: Nighttime
760 isoprene chemistry at an urban-impacted forest site, Journal of Geophysical Research:
761 Atmospheres, 103, 22437-22447, 10.1029/98JD01201, 1998.
- 762 Su, L., Patton, E. G., Vilà-Guerau de Arellano, J., Guenther, A. B., Kaser, L., Yuan, B., Xiong, F.,
763 Shepson, P. B., Zhang, L., Miller, D. O., Brune, W. H., Baumann, K., Edgerton, E., Weinheimer, A.,
764 and Mak, J. E.: Understanding isoprene photo-oxidation using observations and modelling over



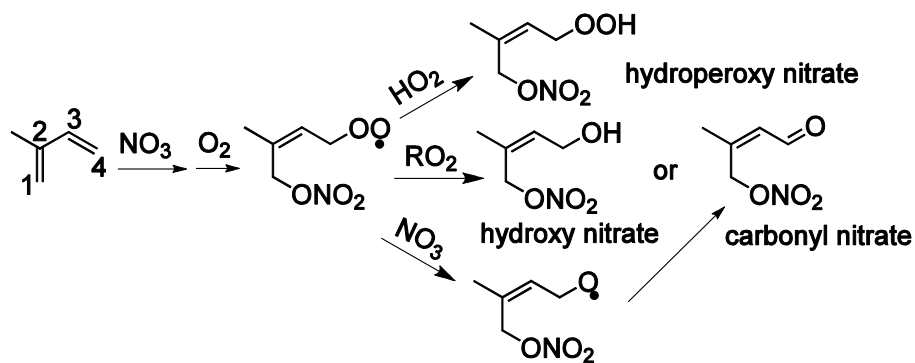
- 765 a subtropical forest in the Southeast US, Atmos. Chem. Phys. Discuss., 15, 31621-31663,
766 10.5194/acpd-15-31621-2015, 2015.
- 767 Suarez-Bertoa, R., Picquet-Varrault, B., Tamas, W., Pangui, E., and Doussin, J. F.: Atmospheric
768 fate of a series of carbonyl nitrates: photolysis frequencies and OH-oxidation rate constants,
769 Environmental science & technology, 46, 12502-12509, 10.1021/es302613x, 2012.
- 770 Treacy, J., Hag, M. E., O'Farrell, D., and Sidebottom, H.: Reactions of Ozone with Unsaturated
771 Organic Compounds, Berichte der Bunsengesellschaft für physikalische Chemie, 96, 422-427,
772 10.1002/bbpc.19920960337, 1992.
- 773 Tuazon, E. C., Atkinson, R., Mac Leod, H., Biermann, H. W., Winer, A. M., Carter, W. P. L., and
774 Pitts, J. N.: Yields of glyoxal and methylglyoxal from the nitrogen oxide(NOx)-air
775 photooxidations of toluene and m- and p-xylene, Environmental science & technology, 18, 981-
776 984, 10.1021/es00130a017, 1984.
- 777 Tuazon, E. C., and Atkinson, R.: A product study of the gas-phase reaction of Isoprene with the
778 OH radical in the presence of NOx, International Journal of Chemical Kinetics, 22, 1221-1236,
779 10.1002/kin.550221202, 1990.
- 780 Vingarzan, R.: A review of surface ozone background levels and trends, Atmospheric
781 Environment, 38, 3431-3442, <http://dx.doi.org/10.1016/j.atmosenv.2004.03.030>, 2004.
- 782 Wang, X., Wang, T., Yan, C., Tham, Y. J., Xue, L., Xu, Z., and Zha, Q.: Large daytime signals of
783 N2O5 and NO3 inferred at 62 amu in a TD-CIMS: chemical interference or a real atmospheric
784 phenomenon?, Atmos. Meas. Tech., 7, 1-12, 10.5194/amt-7-1-2014, 2014.
- 785 Wiberg, K. B., Hadad, C. M., Rablen, P. R., and Cioslowski, J.: Substituent effects. 4. Nature of
786 substituent effects at carbonyl groups, Journal of the American Chemical Society, 114, 8644-
787 8654, 10.1021/ja00048a044, 1992.
- 788 Wu, S., Mickley, L. J., Jacob, D. J., Logan, J. A., Yantosca, R. M., and Rind, D.: Why are there large
789 differences between models in global budgets of tropospheric ozone?, Journal of Geophysical
790 Research: Atmospheres, 112, D05302, 10.1029/2006JD007801, 2007.
- 791 Xie, Y., Paulot, F., Carter, W. P. L., Nolte, C. G., Luecken, D. J., Hutzell, W. T., Wennberg, P. O.,
792 Cohen, R. C., and Pinder, R. W.: Understanding the impact of recent advances in isoprene
793 photooxidation on simulations of regional air quality, Atmospheric Chemistry and Physics, 13,
794 8439-8455, 10.5194/acp-13-8439-2013, 2013.
- 795 Xiong, F., McAvey, K. M., Pratt, K. A., Groff, C. J., Hostetler, M. A., Lipton, M. A., Starn, T. K.,
796 Seeley, J. V., Bertman, S. B., Teng, A. P., Crounse, J. D., Nguyen, T. B., Wennberg, P. O., Misztal,
797 P. K., Goldstein, A. H., Guenther, A. B., Koss, A. R., Olson, K. F., de Gouw, J. A., Baumann, K.,
798 Edgerton, E. S., Feiner, P. A., Zhang, L., Miller, D. O., Brune, W. H., and Shepson, P. B.:
799 Observation of isoprene hydroxynitrates in the southeastern United States and implications for
800 the fate of NOx, Atmos. Chem. Phys., 15, 11257-11272, 10.5194/acp-15-11257-2015, 2015.



801 Zellner, R., and Lorenz, K.: Laser photolysis/resonance fluorescence study of the rate constants
802 for the reactions of hydroxyl radicals with ethene and propene, The Journal of Physical
803 Chemistry, 88, 984-989, 10.1021/j150649a028, 1984.
804

805 List of Figures

806
807 Figure 1. Organic nitrates produced from NO₃-initiated isoprene oxidation.
808 Figure 2. The synthesis route for the 4,1-isoprene carbonyl nitrate.
809 Figure 3. UV absorption cross section of the carbonyl nitrate, MACR and isopropyl nitrate. The
810 spectra were obtained in acetonitrile solvent.
811 Figure 4. Theoretical absorption spectra of the carbonyl nitrate, MACR, and *n*-butyl nitrate in the
812 gas phase.
813 Figure 5. Molecular orbital analysis of the first (a) and second (b) electronic excitation of the
814 carbonyl nitrate. The blue and red colors represent the opposite phases of molecular orbitals.
815 Figure 6. Wall loss and photolysis loss of the carbonyl nitrate in the reaction chamber.
816 Figure 7. The radiation spectra of the chamber (red) and the sun (green, SZA=45° as an example),
817 and the absorption spectra of the carbonyl nitrate (black) and chlorine (blue).
818 Figure 8. The first-order loss of propene relative to that of the carbonyl nitrate for OH-initiated (a)
819 and O₃-initiated (b) oxidation reactions.
820 Figure 9. The relative contributions of photolysis (orange), OH oxidation (green) and O₃
821 oxidation (blue) to the photochemical decay of the carbonyl nitrate, calculated based on
822 measured OH and O₃ concentrations for the following field studies: BERLIOZ 1998 study at
823 Pabstthum, Germany (Mihelcic et al., 2003; Platt et al., 2002), HUMPPA-COPEC 2010 study at
824 Hyytiälä, Finland, SOS 1999 study at Nashville, US (Martinez et al., 2003; Roberts et al., 2002)
825 and PRIDE-PRD 2006 study at Guangzhou, China (Lu et al., 2012).
826 Figure 10. The CIMS spectra before (red) and after (black) the OH + carbonyl nitrate oxidation
827 reaction. The inverted triangles show the decreases in CIMS signals for the carbonyl nitrate (m/z
828 272) and the NO₃⁻ fragments (m/z 62, water cluster at m/z 80) derived from the carbonyl nitrate
829 (Fig. 11).
830 Figure 11. A proposed reaction mechanism for the H abstraction pathway for the OH + carbonyl
831 nitrate oxidation reaction. The compounds in boxes are proposed products as observed by the
832 CIMS (Fig. 8).
833 Figure 12. Proposed reaction mechanisms for OH addition to the C2 (a) and C3 (b) position of
834 the carbonyl nitrate. The compounds in boxes are proposed products as observed by the CIMS
835 (Fig. 8).
836 Figure 13. The GC-ECD/CIMS spectra for the carbonyl nitrate (red), MVK nitrate (blue) and
837 ethanal nitrate (green). The reaction of iodide with the carbonyl nitrate generated NO₃⁻ ion
838 (orange). The ECD chromatogram is shown in black.
839 Figure 14. The formation of ethanal nitrate (a) and MVK nitrate (b) relative to the loss of the
840 isoprene carbonyl nitrate for the OH + carbonyl nitrate oxidation experiments.
841 Figure 15. CIMS spectra before (red) and after (black) the photolysis of the isoprene carbonyl
842 nitrate.
843 Figure 16. A proposed reaction mechanisms for the carbonyl nitrate photolysis reaction. The
844 compounds in boxes are proposed products as observed by the CIMS (Fig. 13).



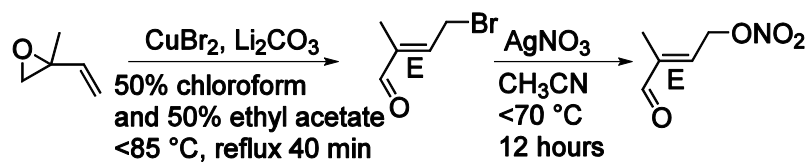
845

846 Figure 1. Organic nitrates produced from NO_3 -initiated isoprene oxidation.

847

848

849

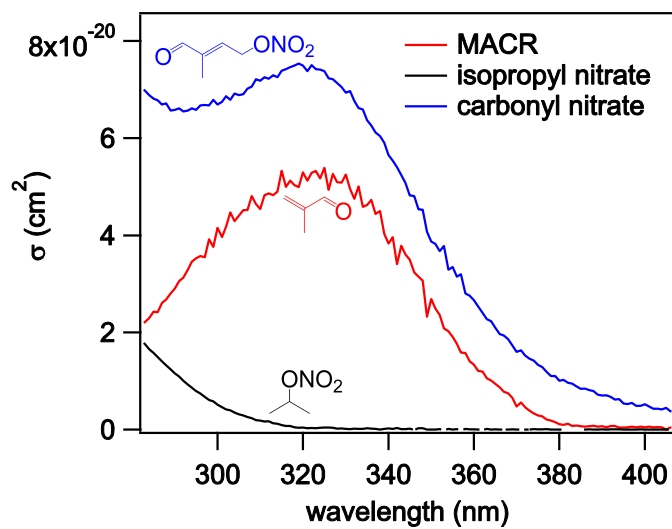


850

851 Figure 2. The synthesis route for the 4,1-isoprene carbonyl nitrate.

852

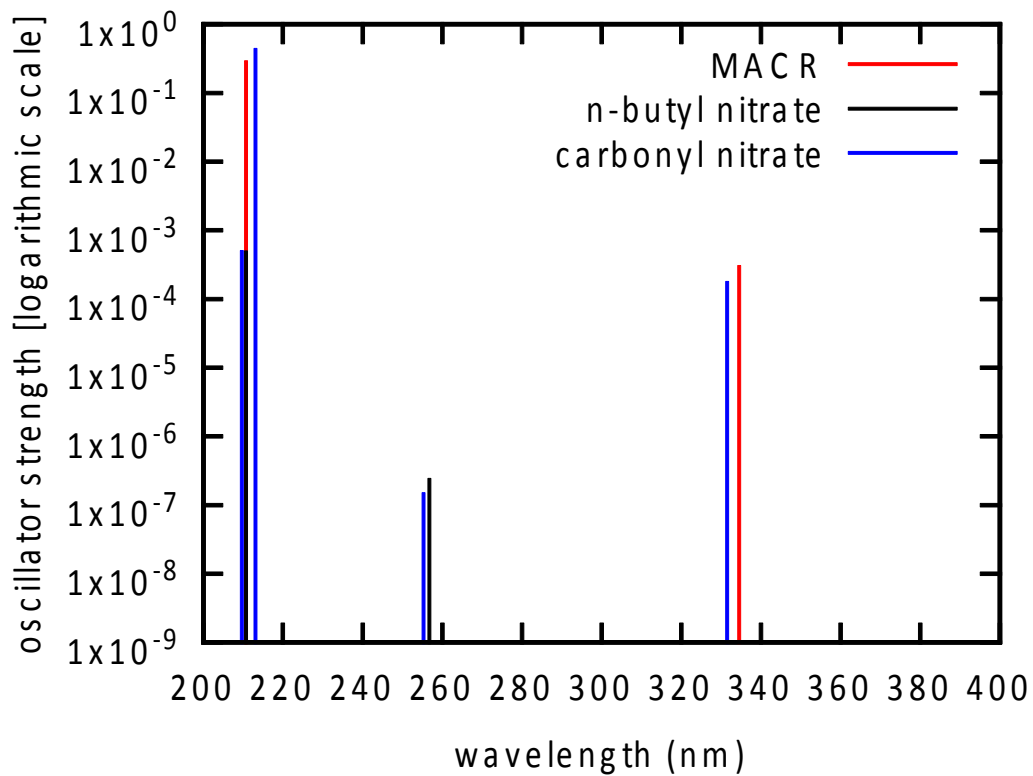
853



854

855 Figure 3. UV absorption cross section of the carbonyl nitrate, MACR and isoproyl nitrate. The
856 spectra were obtained in acetonitrile solvent.

857



858

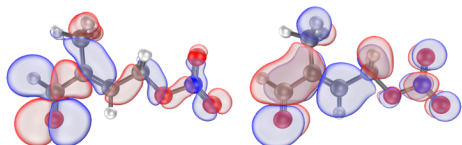
859 Figure 4. Theoretical absorption spectra of the carbonyl nitrate, MACR, and *n*-butyl nitrate in the
860 gas phase.

861

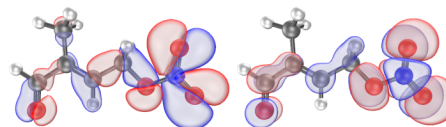
862



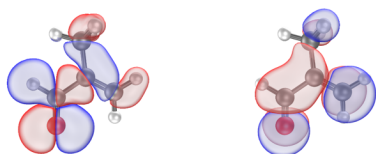
(a) First excitation in carbonyl nitrate
331.51 nm \approx 3.7404 eV
HOMO \rightarrow LUMO



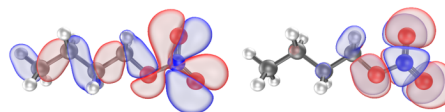
(b) Second excitation in carbonyl nitrate
255.27 nm \approx 4.8575 eV
HOMO-2 \rightarrow LUMO+1



Homologous excitation in MACR
334.54 nm \approx 3.7066 eV
HOMO \rightarrow LUMO



Homologous excitation in *n*-butyl nitrate
256.76 nm \approx 4.8295 eV
HOMO \rightarrow LUMO

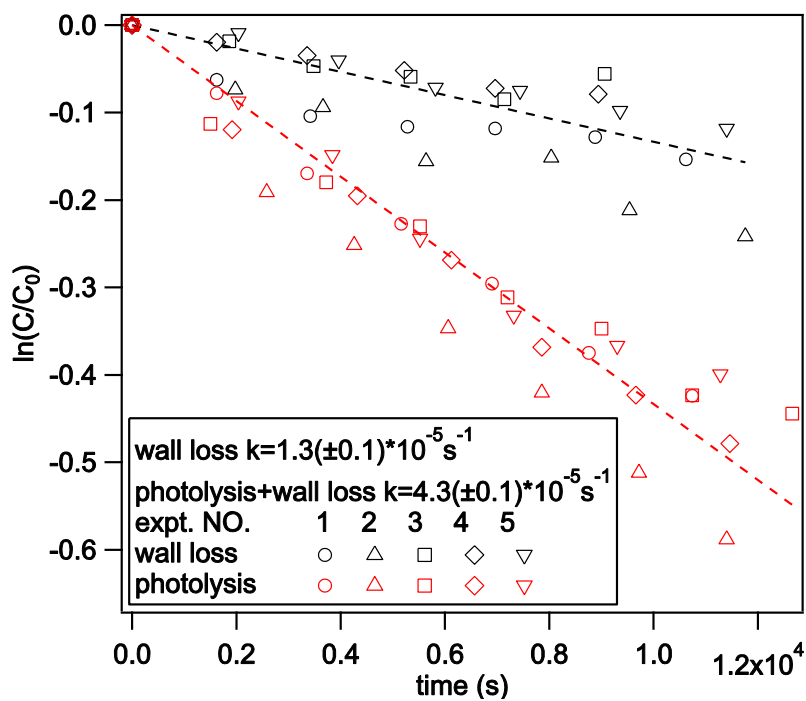


863

864 Figure 5. Molecular orbital analysis of the first (a) and second (b) electronic excitation of the
865 carbonyl nitrate. The blue and red colors represent the opposite phases of molecular orbitals.

866

867

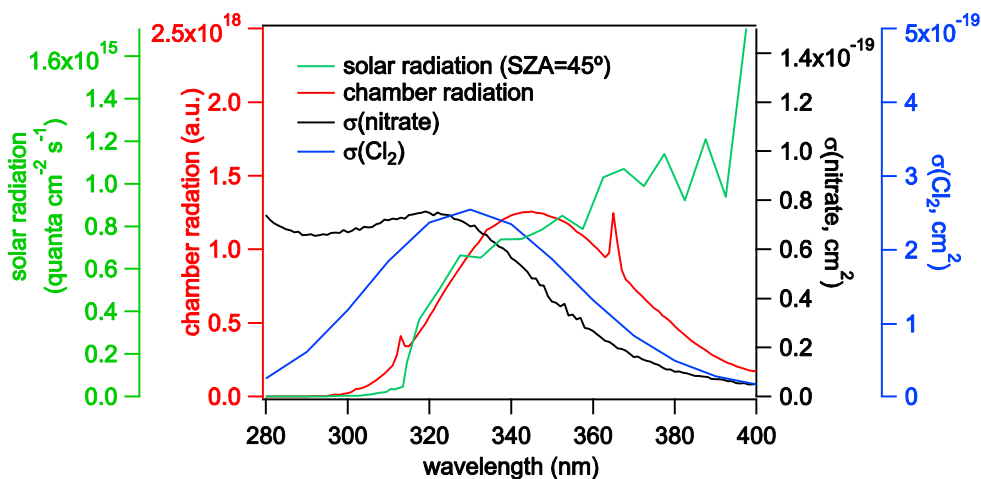


868

869 Figure 6. Wall loss and photolysis loss of the carbonily nitrate in the reaction chamber.

870

871

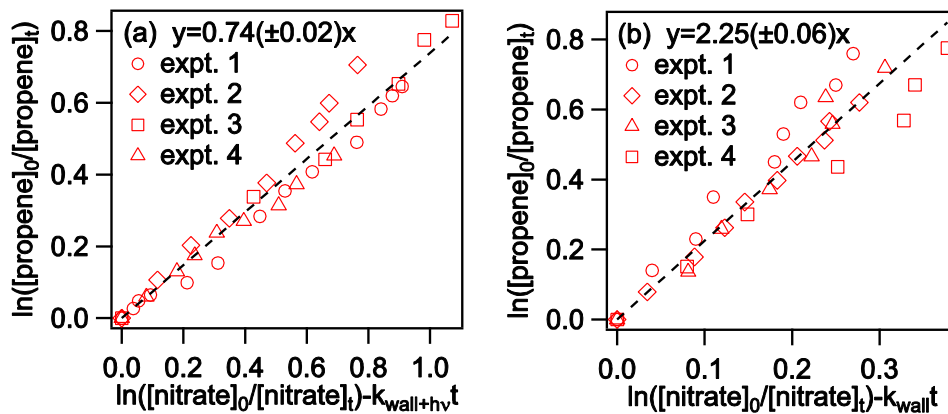


872

873 Figure 7. The radiation spectra of the chamber (red) and the sun (green, SZA=45° as an example),
874 and the absorption spectra of the carbonyl nitrate (black) and chlorine (blue).

875

876



877

878 Figure 8. The first-order loss of propene relative to that of the carbonyl nitrate for OH-initiated (a)
879 and O₃-initiated (b) oxidation reactions.

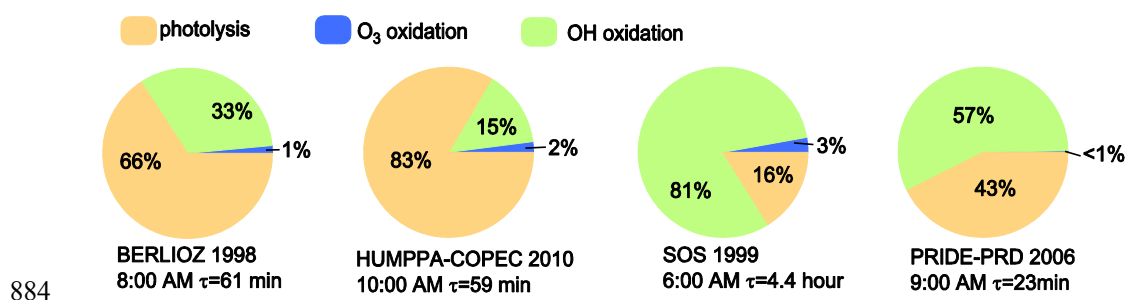
880



881

882

883

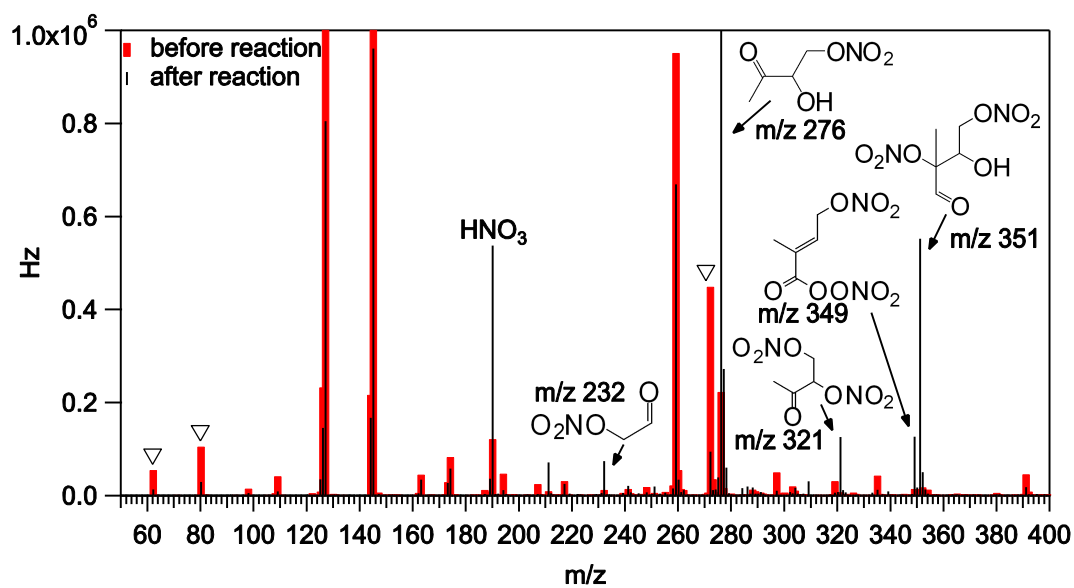


884

885 Figure 9. The relative contributions of photolysis (orange), OH oxidation (green) and O₃
886 oxidation (blue) to the photochemical decay of the carbonyl nitrate, calculated based on
887 measured OH and O₃ concentrations for the following field studies: BERLIOZ 1998 study at
888 Pabstthum, Germany (Platt et al., 2002; Mihelcic et al., 2003), HUMPPA-COPEC 2010 study at
889 Hyytiälä, Finland, SOS 1999 study at Nashville, US (Roberts et al., 2002; Martinez et al., 2003)
890 and PRIDE-PRD 2006 study at Guangzhou, China (Lu et al., 2012).

891

892

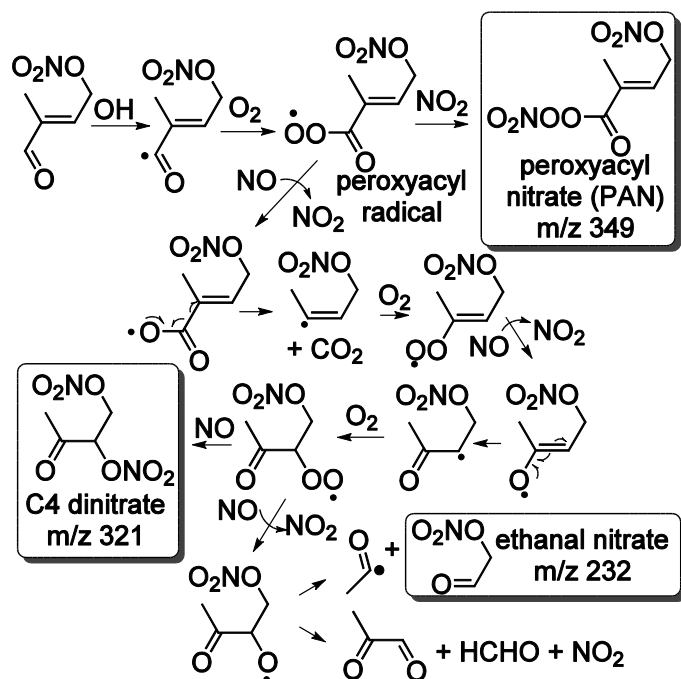


893

894 Figure 10. The CIMS spectra before (red) and after (black) the OH + carbonyl nitrate oxidation
895 reaction. The inverted triangles show the decreases in CIMS signals for the carbonyl nitrate (m/z
896 272) and the NO_3^- fragments (m/z 62, water cluster at m/z 80) derived from the carbonyl nitrate
897 (Fig. 11).

898

899



900

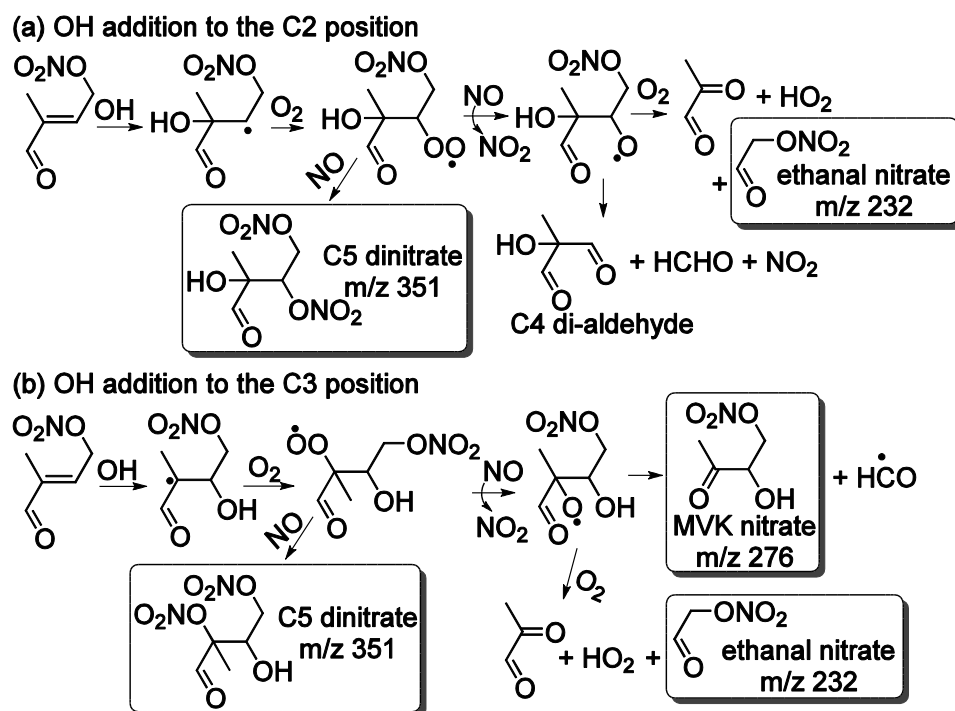
901 Figure 11. A proposed reaction mechanism for the H abstraction pathway for the OH + carbonyl
902 nitrate oxidation reaction. The compounds in boxes are proposed products as observed by the
903 CIMS (Fig. 8).

904

905



906

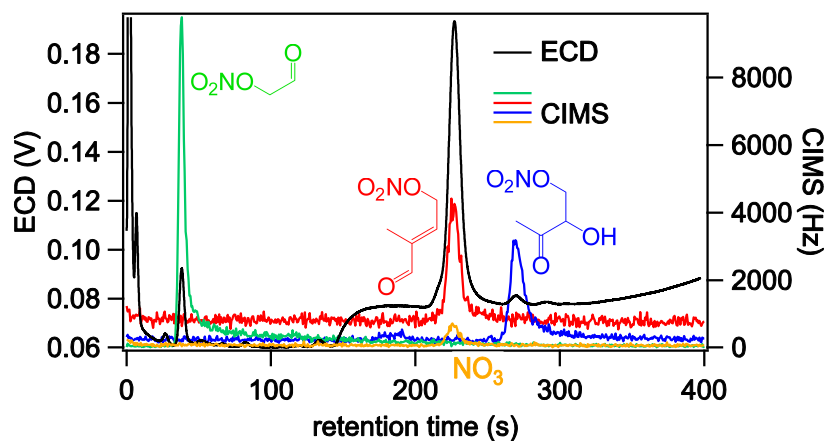


907

908 Figure 12. Proposed reaction mechanisms for OH addition to the C2 (a) and C3 (b) position of
 909 the carbonyl nitrate. The compounds in boxes are proposed products as observed by the CIMS
 910 (Fig. 8).

911

912

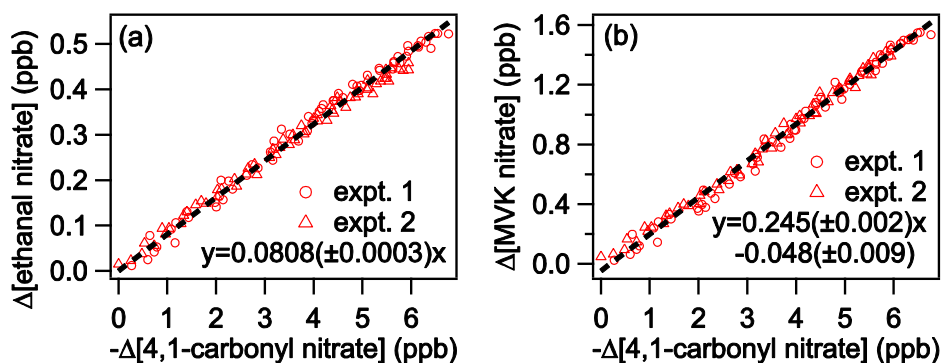


913

914 Figure 13. The GC-ECD/CIMS spectra for the carbonyl nitrate (red), MVK nitrate (blue) and
915 ethanal nitrate (green). The reaction of iodide with the carbonyl nitrate generated NO_3^- ion
916 (orange). The ECD chromatogram is shown in black.

917

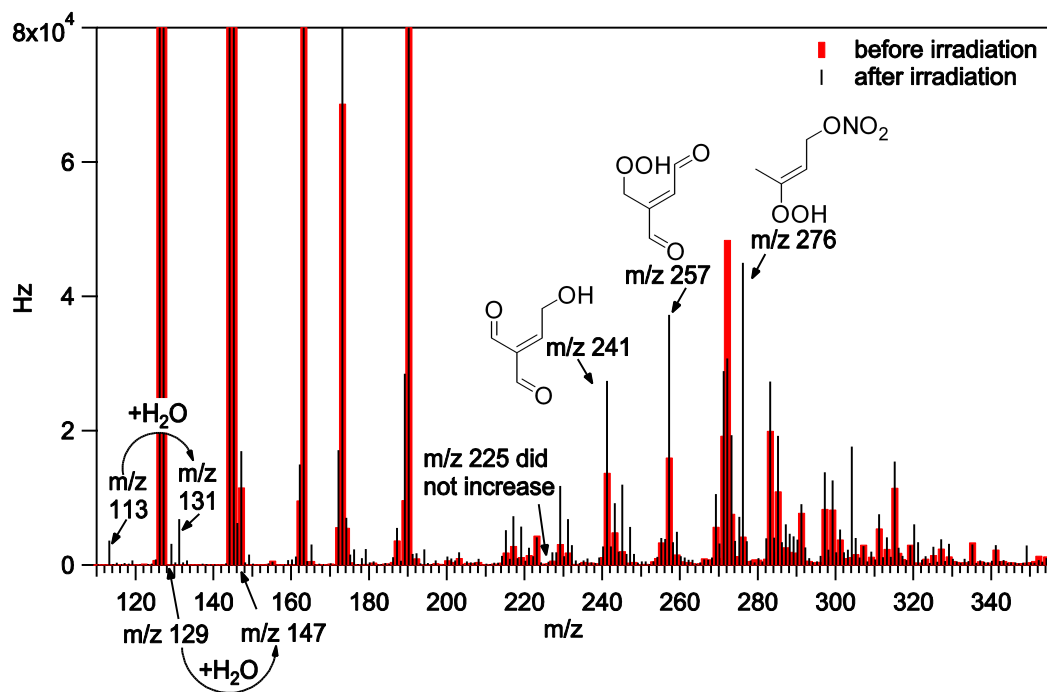
918



919

920 Figure 14. The formation of ethanal nitrate (a) and MVK nitrate (b) relative to the loss of the
921 isoprene carbonyl nitrate for the OH + carbonyl nitrate oxidation experiments.

922

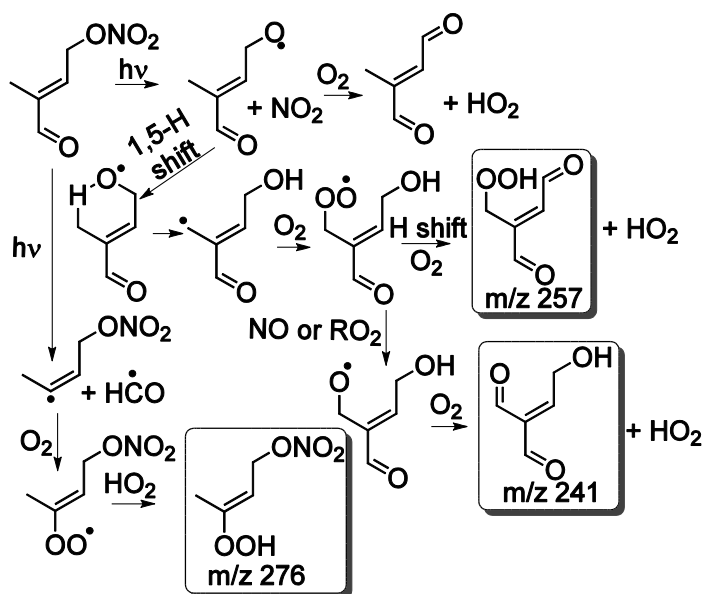


923

924 Figure 15. CIMS spectra before (red) and after (black) the photolysis of the isoprene carbonyl
925 nitrate.

926

927



928

929 Figure 16. A proposed reaction mechanisms for the carbonyl nitrate photolysis reaction. The
930 compounds in boxes are proposed products as observed by the CIMS (Fig. 13).

931